AUT Journal of Modeling and Simulation

AUT J. Model. Simul., 57(1) (2025) 29-52
DOI: 10.22060/miscj.2025.23244.5361

Robust Model Predictive Terminal Guidance Law Using Laguerre Functions

Mohammad Sadegh Nazari, Saeed Nasrollahi*

Faculty of Electrical and Computer Engineering, Malek Ashtar University of Technology, Tehran, Iran.

ABSTRACT: This paper presents a new approach for guiding a pursuer to intercept a maneuvering target in two dimensions. This robust nonlinear approach is based on the combination of predictive control and sliding mode control. The guidance strategy uses a model predictive control method based on the Laguerre function to calculate the pursuer's acceleration command independently of the target's acceleration. To handle unknown target maneuvers, a sliding mode term is added to adjust to the target's acceleration commands, making the algorithm more robust against uncertainties and improving its ability to pursue maneuvering targets effectively. The proposed guidance algorithm was extensively tested through simulations with various target maneuvers, including non-maneuvering, step maneuvers, sinusoidal maneuvers, and stochastic maneuvers. A detailed comparison was made with traditional methods like proportional navigation, ant colony optimization-based predictive control, proportional guidance with a bias switch, and a square programming approach based on differential game theory. Additionally, to observe the effect of the design parameters in the proposed guidance law, a sensitivity analysis is done on the convergence of the pursuer acceleration and the line-of-sight rate. Finally, the influence of disturbances was investigated by adjusting the target acceleration parameter to 10%, 20%, 30%, 50%, 75%, and 100% beyond the maximum value.

Review History:

Received: Jun. 02, 2024
Revised: Jul. 26, 2025
Accepted: Aug. 03, 2025
Available Online: Aug. 05, 2025

Keywords:

Model Predictive Guidance Law
Laguerre Functions
Sliding Mode Control
Maneuvering Target
Stochastic Maneuver

1- Introduction

A guidance subject is defined as finding the commands to steer a pursuer to the desired path. The guidance phases of a pursuer are usually divided into boost, midcourse, and terminal [1]. There are various design methods for the terminal phase guidance law, including proportional navigation guidance developed extensively due to its simple design and implementation[2–4]. Despite its good performance against non-maneuvering targets, it performs poorly against maneuvering targets. The improved proportional navigation method is somewhat robust to maneuvering targets [5] given the target's acceleration, but ineffective against targets with high maneuver [6,7]. Numerous methods have been proposed to improve the guidance law against maneuvering targets, most of which estimate the target's maneuver using different approaches. They also require a target estimator, which increases computational burden and the likelihood of target estimation error due to insufficient information about the kinematics of the engagement. Nonlinear control methods are often used to make the guidance law robust to the target's maneuver. Sliding mode control (SMC) is a widely used control method in systems with uncertainty [8–11]. In [12], second-order sliding mode control has been used to engage maneuvering targets and used smoothing to eliminate chattering, which is also employed in the integrated missile guidance and control system [13]. Also, in [14], a second-order sliding mode control algorithm has been proposed to intercept maneuvering targets and eliminate chattering with a low-pass filter. A sliding mode observer has been used to estimate the target's maneuver while reducing target estimation complexity with the Kalman filter. In [15], a sliding mode control has been investigated to design and improve the guidance law with a modified saturation function based on adaptive laws. In [16,17], a sliding mode control has been considered where the zero effort miss distance is considered as the sliding surface. In [18], a robust guidance method based on zero effort miss distance has been presented to engage maneuvering targets, and proposed a new function to properly estimate time to go. Likewise, robust control methods [19,20] H_∞, the Lyapunov function approach [21,22], and linear feedback controllers were used [23,24] to engage maneuvering targets.

The proportional navigation guidance law and nonlinear guidance laws, which are mentioned above, do not consider guidance acceleration constraints when designing the guidance law. Although the acceleration command in proportional navigation can assume any value without restrictions, this assumption is not strictly true due to practical

*Corresponding author's email: nasrollahi.saeid@gmail.com

system limitations. For example, the system has limited acceleration tolerance; actuators have a limited range to apply the acceleration command, sensors can measure values within a specific range, or system variables have upper and lower limits that cannot be exceeded, fearing system damage or malfunction [25]. In these methods, after exceeding the permitted range with the acceleration command, the control program will impose the maximum value. This method does not guarantee an optimal acceleration command, and increasing it to the saturation state in closed-loop systems may cause instability with limited input control. Therefore, considering the limitations in the design stage is very important and is one of the key points in designing constrained systems. One method that can consider design constraints is the predictive control method[26,27].

Recent developments in the model predictive control and information processing have made this method applicable to systems with fast [28,29] and unstable dynamics [30]. Improved system robustness to uncertainty [31] and simplification and reduction of computational burden [32] have made this method applicable to airborne [33] and aerospace systems. A combination of the model predictive control and the robust control provides a powerful guidance law for nonlinear guidance problems with unknown target maneuvers. In [34], a robust model predictive guidance law based on linear covariance has been proposed. First, the closed-loop covariance method estimates the expected errors of the nominal state variables in case of uncertainty and uses them as part of the cost function to ensure the system's robustness. Then, the predictive control method optimally solves the guidance problem. In [35], a robust predictive control method based on neural networks has been presented for solving the constrained problem. Due to its computational burden, this method is ill-suited for systems with slow processors. In [36], a robust predictive guidance law has been investigated that uses an explicit linear design for solving nonlinear optimization and uses the modified robust L1 navigation law to ensure the robust guidance problem can be solved. In [37], a nonlinear model predictive guidance algorithm with a disturbance observer has been designed according to the system's dynamic limitations. In [38], a heuristic nonlinear model predictive terminal guidance algorithm has been presented that uses an ant colony optimization algorithm to estimate pursuit states, target maneuvers, and optimal guidance commands simultaneously. Despite uncertainties, In [39], a nonlinear robust model predictive guidance algorithm based on a particle swarm optimization algorithm has been presented to solve the problem of two-dimensional engagement of a pursuer and a maneuvering target affected by matched uncertainties. An uncertain guidance problem is converted into a model predictive control problem by introducing an appropriate objective function that reflects the uncertainty. In [40], a robust predictive model for convex programming for nonlinear missile and aircraft landing guidance has been proposed. In this method, a convex optimization framework for the cost function is used to consider inequality constraints and a sensitivity relationship between states and inputs. A limitation of this technique is that increasing the prediction horizon exponentially increases computations. Despite its numerous advantages, the integral predictive control method is computationally burdensome, which could be challenging for real-time and practical implementation [41].

In [42] a predictive guidance method in the midcourse phase based on orthogonal Legendre functions is introduced. In this method, an interceptor midcourse guidance problem with an angle constraint is formulated and solved to intercept an incoming ballistic missile target. Although the computational burden of this method is less than the GPC method, there is no limitation on the guidance command, and there is no ability to track maneuver targets if used in the terminal phase

The implementation of the predictive control method is one of the important parts of using this controller in the industry. In [43] it has been done to check the hardware implementation of the controller on the simulator of hydraulic press machines. It was also implemented in an Embedded system [44]. This method has also been implemented in the aerospace system [45]. The implementation of the Laguerre predictive control method to guide a flying object with the ability to track maneuvering targets has been done in the proposed article.

In this paper, a novel control strategy combining Model Predictive Control (MPC) with Laguerre functions and Sliding Mode Control (SMC) is presented. The MPC framework is employed to systematically handle system constraints, particularly addressing physical limitations such as actuator saturation in practical implementations. The Laguerre function approach is adopted to reduce computational complexity through efficient control input parameterization, enabling real-time applications. Furthermore, SMC is incorporated to enhance system robustness against uncertainties, specifically treating target acceleration as bounded disturbances. This integrated methodology effectively combines the complementary advantages of both control techniques, offering a theoretically rigorous and practically viable solution for complex control challenges. The contribution of the current study is summarized as follows: a constraint guidance law for nonlinear engagement of a pursuer and a target using a combination of model predictive control based on Laguerre's functions and the sliding mode control has been proposed to utilize the strengths of both methods. The dynamic model of the pursuer autopilot is considered as a first-order lag. To use model predictive control, the pursuer and target engagement equations were linearized at the operating point. The linearized state-space model was used to calculate the optimal Laguerre gain, and the guidance command was applied to the nonlinear model. Also, the sliding mode term has been added to the guidance command to engage maneuvering targets. Here, the target maneuver is known as a disturbance term its maximum value is specified. To the author's knowledge, the nonlinear guidance problem with autopilot lag and unknown target maneuver has not been solved using a combination of model predictive control

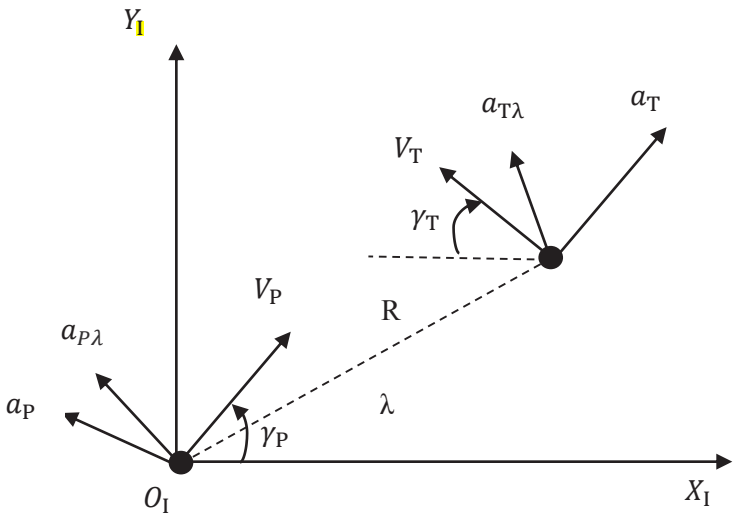

Fig. 1. The Two-Dimensional Model of the Pursuer and Target Kinematics of Engagement

based on Laguerre's functions and the sliding mode control. Performance of the proposed guidance law is evaluated via various numerical simulations and compared to some other approaches.

Some of the problems related to this method and the practical techniques to solve it in this article are as follows:

Linearization should be performed around operating points. To ensure the linear and nonlinear dynamic models remain closely aligned, the system is linearized over short time intervals. However, this increases the computational burden at each time step. To mitigate this issue, the linearization interval can be adjusted such that the linear and nonlinear systems exhibit similar behavior, thereby reducing the frequency of linearization while maintaining accuracy.

The computational volume due to the inversion of the matrices may cause the system to go out of real-time mode. To solve this problem, instead of performing the calculations related to inverting the matrix, the calculations of the inverted matrix can be solved parametrically, and then at each step when inversion is needed, it can only be substantiated in the parametric form.

The rest of the paper is organized as follows. Section 2 describes the mathematical equations governing pursuer and target geometry, Section 3 states the guidance law, and Section 4 presents simulation results and performance of the proposed guidance law. Finally, section 5 presents the conclusion.

2- Problem Definition

This section presents a two-dimensional nonlinear model of pursuer and target kinematics of engagement shown in Fig. 1, where subscript P denotes the pursuer and subscript T denotes the target. The λ angle is the line of sight (LOS) measured relative to the X_I reference, R is the relative distance between the pursuer and the target, and the target velocity vectors are respectively shown with V_P and V_T, respectively. a_P and a_T are respectively the pursuer and target acceleration perpendicular to the velocity vector, and $a_{T\lambda}$ are respectively the pursuer and target acceleration perpendicular to LOS.

The gravitational acceleration has a small acceleration command in the terminal phase. By this assumption, the relative kinematic equations of the pursuer and the target are stated as follows [39]:

$$\dot{R} = -V_T \cos(\lambda + \gamma_T) - V_P \cos(\gamma_P - \lambda) \tag{1}$$

$$\dot{\lambda} = \frac{V_T \sin(\lambda + \gamma_T) - V_P \sin(\gamma_P - \lambda)}{R} \tag{2}$$

$$\dot{\gamma}_P = \frac{a_P}{V_P} \tag{3}$$

$$\dot{\gamma}_T = \frac{a_T}{V_T} \tag{4}$$

In this kinematics of the engagement, $\dot{R} < 0$ and $\dot{\lambda} = 0$ are the target engagement conditions. To obtain the state-space according to the state vector as: $\mathbf{X} = \left[R \ \dot{R} \ \dot{\lambda} \ a_P \ \gamma_P \ \gamma_T \ \lambda \right]$, the R and λ should be derived. The time derivatives of Equations (1) and (2) are as follows:

$$\ddot{R} = R\dot{\lambda}^2 + a_P \sin(\gamma_P - \lambda) + a_T \sin(\gamma_T + \lambda) \tag{5}$$

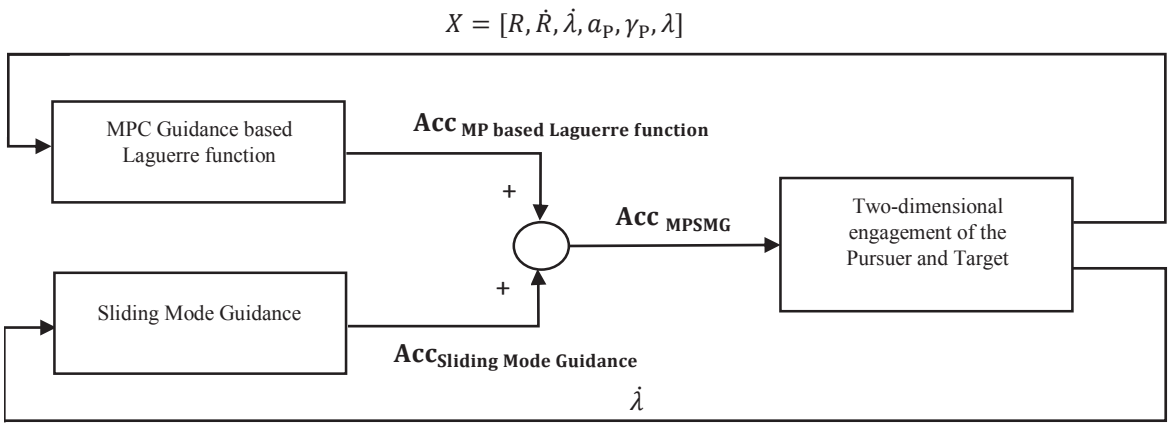

Fig. 2. The Block Diagram of MPSMG Guidance Law.

$$\ddot{\lambda} = \frac{1}{R}(-2\dot{R}\dot{\lambda} - a_{\mathrm{P}}\cos(\gamma_{\mathrm{P}} - \lambda) + a_{\mathrm{T}}\cos(\gamma_{\mathrm{T}} - \lambda)) \quad (6)$$

The dynamic model of the autopilot was considered a first-order model:

$$\dot{a}_{\mathrm{P}} = -\frac{1}{\tau}a_{\mathrm{P}} + \frac{1}{\tau}u \quad (7)$$

where, u is the input of the autopilot, and τ is the time constant of the pursuer. The nonlinear state-space equations are as follows:

$$\dot{x}_1(t) = x_2(t) \quad (8)$$

$$\dot{x}_2(t) = x_1(t)x_3^2(t) + x_4(t)\sin\big(x_5(t) - x_7(t)\big) + a_{\mathrm{T}}\sin(x_6(t) + x_7(t)) \quad (9)$$

$$\dot{x}_3(t) = \frac{1}{x_1(t)}(-2x_2(2)x_3(t) - x_4(t)\cos\big(x_5(t) - x_7(t)\big) + a_{\mathrm{T}}\cos\big(x_6(t) + x_7(t)\big)) \quad (10)$$

$$\dot{x}_4(t) = -\frac{1}{\tau}x_4(t) + \frac{1}{\tau}u \quad (11)$$

$$\dot{x}_5(t) = \frac{x_4(t)}{V_{\mathrm{P}}} \quad (12)$$

$$\dot{x}_6(t) = \frac{a_{\mathrm{T}}}{V_{\mathrm{T}}} \quad (13)$$

$$\dot{x}_7(t) = \frac{V_{\mathrm{T}}\sin\big(x_7(t) + x_6(t)\big) - V_{\mathrm{P}}\sin(x_5(t) - x_7(t))}{x_1(t)} \quad (14)$$

3- Model Predictive Sliding Mode Guidance

This section will obtain the equations related to designing the Model Predictive Sliding Mode Guidance (MPSMG) law in two parts: the first part is based on constraint model predictive guidance using Laguerre functions, and the second part is based on the sliding mode control. The MPSMG guidance law block diagram is as follows. According to Fig. 2, the guidance command is obtained as follows:

$$\mathbf{Acc}_{\mathbf{MPSMG}} = \mathbf{Acc}_{\mathbf{MP}} + \mathbf{Acc}_{\mathbf{SMG}} \quad (15)$$

where, $\mathbf{Acc}_{\mathbf{SMG}} = \rho\, sign(S)$, $S = \dot{\lambda}$ the sliding surface, and $\rho \geq \max(a_{\mathrm{T}})$ is a positive parameter and bounded. The hyperbolic tangent function was used instead of the sign function to eliminate chattering.

3- 1- Model Predictive Guidance Law Using Laguerre Functions

This section presents the constraint model predictive guidance term, $\mathbf{Acc}_{\mathbf{MP}}$, using Laguerre functions. Eqn. (16) defines the difference of the acceleration command vector $\Delta\mathbf{ACC}_{\mathbf{MP}}$ for optimization in the prediction horizon $\mathrm{N_p}$:

$$\Delta\mathbf{ACC}_{\mathbf{MP}} = [\Delta\mathbf{Acc}_{\mathbf{MP}}(\mathrm{k_i})\ \ \Delta\mathbf{Acc}_{\mathbf{MP}}(\mathrm{k_i}+1)\ldots\Delta\mathbf{Acc}_{\mathbf{MP}}(\mathrm{k_i}+\mathrm{N_p}-1)]^{\mathbf{T}} \quad (16)$$

Each element of $\Delta\mathbf{ACC}_{\mathbf{MP}}$ vector in k_i time is expressed in the following Dirac delta function:

$$\Delta\mathbf{Acc}_{\mathbf{MP}}(\mathrm{k_i}+1) = [\boldsymbol{\delta}(\mathrm{i})\ \ \boldsymbol{\delta}(\mathrm{i}-1)\ldots\boldsymbol{\delta}(\mathrm{i}-\mathrm{N_p}+1)]\Delta\mathbf{ACC}_{\mathbf{MP}} \quad (17)$$

The time form of Laguerre functions is shown as the following vector:

$$\mathbf{L}(\mathrm{k}) = [\mathbf{l}_1(\mathrm{k})\ \mathbf{l}_2(\mathrm{k})\ \ldots\ \mathbf{l}_N(\mathrm{k})]^{\mathrm{T}} \tag{18}$$

where vector l is orthogonal and conversion z-1 of Laguerre functions.

$\Delta A\mathbf{cc}_{\mathbf{MP}}(\mathrm{k_i})$, $\Delta A\mathbf{cc}_{\mathbf{MP}}(\mathrm{k_i}+1)$ and… $\Delta A\mathbf{cc}_{\mathbf{MP}}(\mathrm{k_i}+\mathrm{N_p}-1)$ is the step response of the stable dynamic system. The set of Laguerre functions $I_1(m)$, $I_2(m),\ldots I_N(m)$ is considered for system dynamics in the design stage. Hence, the $\Delta A\mathbf{cc}_{\mathbf{MP}}(\mathrm{k_i}+\mathrm{k})=\sum_{j=1}^{N}\boldsymbol{c}_j(\mathrm{k})\mathbf{l}_j(\mathrm{k})$ Dirac delta response can be defined as the following Laguerre functions:

$$\mathbf{\Delta Acc}_{\mathbf{MP}}(\mathrm{k_i}+\mathrm{m}) = \mathbf{L}(\mathrm{k})^{\mathrm{T}}\boldsymbol{\eta} = [\mathbf{l}_1(m)\quad \mathbf{l}_2(m)\ \ldots\ \mathbf{l}_N(m)]\boldsymbol{\eta} \tag{19}$$

The η is the Laguerre function coefficients, $\eta=\left[\mathrm{c}_1\ \ \mathrm{c}_2\ \ldots\ \mathrm{c}_{\mathrm{N}}\right]^{\mathrm{T}}$. Appendix A completely proves the differential acceleration command in terms of Laguerre functions.

The Linear Quadratic Regulator (LQR) method was used to optimize the guidance command, where the input is zero, the output is the signal error, and optimization is aimed at minimizing the squared errors to determine state coefficients. Stability can be evaluated using this well-known method. To test the LQR method's stability, the prediction horizon is set to infinite, and the problem is considered unconstrained [46]. $\mathbf{x}(\mathrm{k_i}+\mathrm{m}|\mathrm{k_i})$ is considered as state vector, Q, and $\mathbf{R}_{\mathrm{L}}$ are weight matrices used in the design to adjust the model. Considering the $\mathbf{Q}=\mathbf{C}^{\mathrm{T}}\mathbf{C}$, the two expressions in Eqn. (20) will be similar to the cost function. The first expression represents the prediction method's cost function, and the second represents the LQR objective function.

$$\mathbf{J} = \sum_{m=1}^{\mathrm{N_p}} \boldsymbol{x}(\mathrm{k_i}+\mathrm{m}|\mathrm{k_i})^{\mathrm{T}}\,\boldsymbol{Q}\boldsymbol{x}(\mathrm{k_i}+\mathrm{m}|\mathrm{k_i}) + \boldsymbol{\eta}^{\mathrm{T}}\boldsymbol{R}_L\boldsymbol{\eta} \tag{20}$$

Thus, the new states are defined as (21).

$$\mathbf{x}(\mathrm{k_i}) = [\mathbf{\Delta x_m}(\mathrm{k_i})^{\mathrm{T}}\quad \mathbf{Acc_{MP}}(\mathrm{k_i})]^{\mathrm{T}} \tag{21}$$

In the new equation defined for states, instead of considering only the output, an error is also considered:

$$\mathbf{x}(\mathrm{k_i}+\mathrm{m}|\mathrm{k_i}) = [\mathbf{\Delta x_m}(\mathrm{k_i}+\mathrm{m}|\mathrm{k_i})^{\mathrm{T}}\quad \mathbf{Acc_{MP}}(\mathrm{k_i}+\mathrm{m}|\mathrm{k_i})-\mathbf{r}(\mathrm{k_i})]^{\mathrm{T}} \tag{22}$$

The predictive equation on the prediction horizon is rewritten as follows:

$$\mathbf{x}(\mathrm{k_i}+\mathrm{m}|\mathrm{k_i}) = \mathbf{A}^m\mathbf{x}(\mathrm{k_i}) + \sum_{i=0}^{m-1}\mathbf{A}^{m-i-1}\,\mathbf{BL}(\mathrm{i})^{\mathrm{T}}\boldsymbol{\eta} = \mathbf{A}^m\mathbf{x}(\mathrm{K_i}) + \boldsymbol{\phi}(\mathrm{m})^{\mathrm{T}}\boldsymbol{\eta} \tag{23}$$

where the ϕ matrix is defined as (24).

$$\boldsymbol{\phi}(\mathrm{m})^{T} = \sum_{i=0}^{m-1}\mathbf{A}^{m-i-1}\mathbf{BL}(\mathrm{i})^{\mathrm{T}} \tag{24}$$

The cost function is rewritten according to the ϕ.

$$\mathbf{J} = \boldsymbol{\eta}^{\mathrm{T}}\sum_{m=1}^{N_p}\boldsymbol{\phi}(m)\mathbf{Q}\boldsymbol{\phi}(\mathrm{m})^{\mathrm{T}} + \mathbf{R}_L)\boldsymbol{\eta} + 2\boldsymbol{\eta}^{\mathrm{T}}(\sum_{m=1}^{N_p}\boldsymbol{\phi}(\mathrm{m})\mathbf{Q}\mathbf{A}^m\mathbf{x}(\mathrm{k_i}) + \sum_{m=1}^{N_p}\mathbf{x}(\mathrm{k_i})(\mathbf{A}^{\mathrm{T}})^m\mathbf{Q}\mathbf{A}^m\mathbf{x}(\mathrm{k_i}) \tag{25}$$

To obtain $\boldsymbol{\eta}$, it is derived from the cost function obtained according to this parameter.

$$\frac{\partial\mathbf{J}}{\partial\boldsymbol{\eta}} = 2(\sum_{m=1}^{N_p}\boldsymbol{\phi}(\mathrm{m})\mathbf{Q}\boldsymbol{\phi}(\mathrm{m})^{\mathrm{T}} + \mathbf{R}_L)\boldsymbol{\eta} + 2\sum_{m=1}^{N_p}\boldsymbol{\phi}(\mathrm{m})\mathbf{Q}\,\mathbf{A}^{\mathrm{m}})\mathbf{x}(\mathrm{k_i}) \tag{26}$$

Assuming that matrix (27) is invertible, the derivative of the cost function in terms of $\boldsymbol{\eta}$ is zero, and the $\boldsymbol{\eta}$ matrix is

obtained as follows.

$$\sum_{m=1}^{N_p} \boldsymbol{\phi}(\mathrm{m})\mathbf{Q}\boldsymbol{\phi}(\mathrm{m})^{T} + \mathbf{R_L}) \tag{27}$$

$$\boldsymbol{\eta} = -(\sum_{m=1}^{N_p} \boldsymbol{\phi}(\mathrm{m})\mathbf{Q}\boldsymbol{\phi}(\mathrm{m})^{\mathrm{T}} + \mathbf{R}_L)^{-1} \sum_{m=1}^{N_p} \boldsymbol{\phi}(\mathrm{m})\mathbf{Q}\mathbf{A}^{m})\mathbf{x}(\mathrm{k_i}) \tag{28}$$

Thus, the Laguerre coefficients are obtained by minimizing the cost function. The following expressions can be used for further simplification.

$$\boldsymbol{\Omega} = \sum_{m=1}^{N_p} \boldsymbol{\phi}(\mathrm{m})\mathbf{Q}\boldsymbol{\phi}(\mathrm{m})^{\mathrm{T}} + \mathbf{R}_L$$

$$\boldsymbol{\psi} = \sum_{m=1}^{N_p} \boldsymbol{\phi}(\mathrm{m})\mathbf{Q}\mathbf{A}^{m} \tag{29}$$

$$\boldsymbol{\eta} = -\boldsymbol{\Omega}^{-1}\boldsymbol{\psi}\mathbf{x}(\mathrm{k_i})$$

The minimum cost function based on Laguerre coefficients (η) will be as follows.

$$\mathbf{J} = \boldsymbol{\eta}^{\mathrm{T}} \sum_{m=1}^{N_p} \boldsymbol{\phi}(\mathrm{m})\mathbf{Q}\boldsymbol{\phi}(\mathrm{m})^{\mathrm{T}} + \mathbf{R}_L)\,\boldsymbol{\eta}$$

$$+2\boldsymbol{\eta}^{\mathrm{T}} \sum_{m=1}^{N_p} \boldsymbol{\phi}(\mathrm{m})\mathbf{Q}\mathbf{A}^{m})\mathbf{x}(\mathrm{k_i})$$

$$+ \sum_{m=1}^{N_p} \mathbf{x}(\mathrm{k_i})^{\mathrm{T}}(\mathbf{A}^{\mathrm{T}})^{m}\mathbf{Q}\mathbf{A}^{m}\mathbf{x}(\mathrm{k_i}) = \tag{30}$$

$$(\boldsymbol{\eta} + \boldsymbol{\Omega}^{-1}\boldsymbol{\psi}\mathbf{x}(\mathrm{k_i}))^{\mathrm{T}}\boldsymbol{\Omega}\big(\boldsymbol{\eta} + \boldsymbol{\Omega}^{-1}\boldsymbol{\psi}\mathbf{x}(\mathrm{k_i})\big)$$

$$-\mathbf{x}(\mathrm{k_i})^{\mathrm{T}}\boldsymbol{\psi}^{\mathrm{T}}\boldsymbol{\Omega}^{-1}\boldsymbol{\psi}\mathbf{x}(\mathrm{k_i}) + \sum_{m=1}^{N_p} \mathbf{x}(\mathrm{k_i})^{\mathrm{T}}(\mathbf{A}^{\mathrm{T}})^{m}\mathbf{Q}\mathbf{A}^{m}\mathbf{x}(\mathrm{k_i})$$

By simplifying Eqn. (30), we have:

$$\mathbf{J} = \mathbf{x}(\mathrm{k_i})^{\mathrm{T}}\left(\sum_{m=1}^{N_p} (\mathbf{A}^{\mathrm{T}})^{\mathrm{m}}\mathbf{Q}\mathbf{A}^{\mathrm{m}} - \boldsymbol{\psi}^{\mathrm{T}}\boldsymbol{\Omega}^{-1}\boldsymbol{\psi}\right)\mathbf{x}(\mathrm{k_i}) = \mathbf{x}(\mathrm{k_i})^{\mathrm{T}}\mathbf{P}_{dmpc}\mathbf{x}(\mathrm{k_i}) \tag{31}$$

where $P_{dmpc} = \sum_{m=1}^{N_p} (A^{\mathrm{T}})^{m} Q A^{m} - \psi^{\mathrm{T}}\Omega^{-1}\Psi$. Convolution coefficients are summarized in (32) in terms of Laguerre coefficients.

$$\mathbf{S}_c(\mathrm{m}) = \sum_{i=0}^{m-1} \mathbf{A}^{m-i-1}\mathbf{B}\mathbf{L}(\mathrm{i})^{\mathrm{T}} \tag{32}$$

Due to the problem's complexity, the recursive method is used to calculate the convolution coefficients.

$$\mathbf{L}(k+1) = \mathbf{A}_1\mathbf{L}(K)$$

$$\mathbf{S}_c(\mathrm{m}) = \mathbf{A}\mathbf{S}_c(\mathrm{m}-1) + \mathbf{S}_c(1)(\mathbf{A}_l^{m-1})^{\mathrm{T}} \tag{33}$$

$$\mathbf{S}_c(1) = \mathbf{B}\mathbf{L}(0)^{\mathrm{T}} \quad and \quad \mathrm{m} = 2,3,4,\ldots,\mathrm{N_p}$$

The $\Delta\mathbf{Acc_{MP}}$ is used in the model predictive guidance method, and $\Delta\mathbf{Acc_{MP}}$ is calculated from the Laguerre coefficients (η). The following equations are used to obtain $\Delta\mathbf{Acc_{MP}}$:

$$\boldsymbol{\Delta}\mathbf{Acc_{MP}}(\mathrm{k_i}) = \mathbf{L}(0)^{\mathrm{T}}\boldsymbol{\eta} \tag{34}$$

By considering $\Delta\mathbf{Acc_{MP}}$ as the following equation, the state feedback is given to the system.

$$\boldsymbol{\Delta}\mathbf{Acc_{MP}}(\mathrm{k}) = -\mathbf{k}_{mpc}\mathbf{x}(\mathrm{k}) \tag{35}$$

$$\mathbf{k}_{mpc} = \mathbf{L}(0)^{\mathrm{T}}(\sum_{m=1}^{N_p} \boldsymbol{\phi}(\mathrm{m})\mathbf{Q}\boldsymbol{\phi}(\mathrm{m})^{\mathrm{T}} + \mathbf{R}_L)^{-1} \sum_{m=1}^{N_p} \boldsymbol{\phi}(\mathrm{m})\mathbf{Q}\mathbf{A}^{m}) = \mathbf{L}(0)^{\mathrm{T}}\boldsymbol{\Omega}^{-1}\boldsymbol{\psi} \tag{36}$$

After calculating the variation in the acceleration command, the acceleration command will be applied to the flying object system as Eq. (37):

$$\mathbf{Acc_{MP}}(\mathrm{k}) = \mathbf{Acc_{MP}}(\mathrm{k}-1) + \mathbf{\Delta Acc_{MP}}(\mathrm{k}) \tag{37}$$

In Eq. (37), there is an inherent integrator that causes complete tracking of the guidance command and also eliminates noise and high-frequency oscillations. Therefore, according to Eq. (37), the proposed model predictive guidance law is similar to a linear quadratic regulator; in other words, it is an optimal real-time guidance law. The stability proof of the robust predictive controller based on SMC is given in [47] in section five. It should be noted that the robust predictive controller based on SMC presented in [47] is not based on Laguerre functions, while the proof of stability is comprehensively presented.

3- 2- Stability Proof for Hybrid (MPSMG) Guidance Law

This section provides a formal stability proof for the hybrid Model Predictive Control (MPC) and Sliding Mode Control (SMC) guidance law (MPSMG) using Lyapunov theory. It is understood that for a large prediction horizon and a large N in the Laguerre functions, the optimal control trajectory converges to the underlying optimal control dictated by a continuous-time linear quadratic regulator (LQR) with the same weight matrices Q and R. The cost functions of predictive control and LQR become nearly identical [48,49].

Considering the target acceleration as a perturbation, the pursuer's linearized dynamics are given by:

$$\dot{\mathbf{X}} = \mathbf{AX} + \mathbf{B}(\mathbf{Acc_{MP}} + \mathbf{Acc_{SMG}}) + \mathbf{Da_T} \tag{38}$$

Where, $\mathrm{Acc}_{\mathrm{MP}} = -\mathrm{K}_{\mathrm{mpc}}\,\mathrm{X}$ is the MPC-based acceleration command (Due to the filtering property of the differential guidance command, the optimal signal is ultimately a coefficient of the states and equal to $\dot{K}_{\mathrm{mpc}}$ [49]), $\mathrm{Acc}_{SMG} = \rho \tanh(\frac{S}{\epsilon})$ is the SMC term (with $\rho \geq \max(\mathrm{a_T})$), $\mathrm{a_T}$ is the bounded target maneuver (disturbance).

For sliding term, $S = \dot{\lambda}$ the sliding surface, its time derivative (from engagement kinematics):

$$\dot{S} = \underbrace{\frac{-2\dot{R}\dot{\lambda}}{R}}_{f(\mathbf{x})} - \underbrace{\frac{\cos(\gamma_P - \lambda)}{R}}_{g(\mathbf{x})}\mathbf{Acc_{MP}} + \underbrace{\frac{-\cos(\gamma_P - \lambda)}{R}}_{g(\mathbf{x})}\rho \tanh\left(\frac{S}{\epsilon}\right) + \underbrace{\frac{\cos(\gamma_T + \lambda)}{R}}_{\Delta(\mathbf{x})}a_T \tag{39}$$

The Lyapunov function is considered as follows:

$$\mathrm{V} = \mathbf{X}^T\boldsymbol{P}\,\mathbf{X} + \frac{1}{2}S^2 \tag{40}$$

where $\boldsymbol{P}$ is the solution to the Lyapunov equation for MPC term.

$$\boldsymbol{A}^T\boldsymbol{P} + \boldsymbol{P}\boldsymbol{A} = -\boldsymbol{Q}, \boldsymbol{Q} > 0 \tag{41}$$

To prove stability, the derivative of V must be calculated and found to be negative:

$$\begin{aligned}\dot{V} &= \mathbf{X}^T(\boldsymbol{A}^T\boldsymbol{P} + \boldsymbol{P}\boldsymbol{A})\mathrm{X} \\ &+2\mathbf{X}^T\boldsymbol{P}\boldsymbol{B}\,(\mathbf{Acc_{MP}} + \mathrm{Acc_{SMG}}) + S\dot{S} = \\ &-\mathrm{X^T Q\,X} + 2\mathbf{X}^T\boldsymbol{P}\boldsymbol{B}\,(\mathbf{Acc_{MP}} + \mathrm{Acc_{SMG}}) + S\dot{S}\end{aligned} \tag{42}$$

$2\mathbf{X}^T\boldsymbol{P}\boldsymbol{B}\mathbf{Acc_{MP}}$ in combination with $-\mathbf{X}^T\boldsymbol{Q}\,\mathbf{X}$, it leads to the negative definite expression $\left(-\mathbf{X}^T\boldsymbol{Q}\,\mathbf{X}\right)$, $S\dot{S} = S\left[f(x) + g(x)\left(-\dot{K}_{mpc}\,\mathbf{X} + \rho\tanh(\frac{S}{\epsilon})\right) + \Delta(x)a_T\right]$.

For $\rho \geq \max|\mathrm{a_T}| + \eta$, and small ϵ; $S\dot{S} \leq -\eta|\mathrm{S}|$ and $2\mathbf{X}^T\boldsymbol{P}\boldsymbol{D}a_T$ is dominated by $S\dot{S}$.

Final Inequality is as follows:

$$\dot{\mathrm{V}} \leq -\mathrm{X^T\dot{Q}\,X} - \eta\,|\mathrm{S}| < 0 \;\text{ for } \forall\, \mathrm{X} \neq 0, \mathrm{S} \neq 0 \tag{43}$$

Therefore, the stability condition of the hybrid method is as follows:

- For MPC: $\dot{Q} \geq 0$, (A, B) stabilizable.
- For SMC: $\rho \geq \max|\mathrm{a_T}| + \eta,\ \ \epsilon > 0$

3- 3- Constrained Model Predictive Guidance Law Using Laguerre Functions

Structural and velocity constraints lead to constraints on maximum, minimum, and acceleration command changes, which are expressed as follows:

$$\begin{aligned}&\mathbf{Acc}_{min} \leq \mathbf{Acc} \leq \mathbf{Acc}_{min} \\ &\mathbf{\Delta Acc}_{min} \leq \mathbf{Acc}(\mathrm{k}) - \mathbf{Acc}(\mathrm{k}-1) \leq \mathbf{\Delta Acc}_{max} \quad \forall k\end{aligned} \tag{44}$$

Now, to consider the constraints in the cost function, they must be defined as the matrix inequality, $M\,\Delta u_{k-1} \leq N$ where the matrices **M** and **N** are defined as follows.

$$\mathbf{M} = \begin{bmatrix}\mathbf{T} \\ -\mathbf{T} \\ \mathbf{I} \\ -\mathbf{I}\end{bmatrix}, \mathbf{N} = \begin{bmatrix}\mathbf{1}u_{max} - \mathbf{Acc}(\mathrm{k}-1)\mathbf{1} \\ -\mathbf{1}u_{min} + \mathbf{Acc}(\mathrm{k}-1)\mathbf{1} \\ \mathbf{1}\,\mathbf{\Delta Acc}_{max} \\ -\mathbf{1}\,\mathbf{\Delta Acc}_{min}\end{bmatrix} \tag{45}$$

where $\mathbf{1}$ is a vector with n_u entries and $\mathbf{T}_{n_u \times n_u}$ is a low triangular matrix with unit value.

Table 1. Comparison of computation time in per iteration in different methods

Computational Method	Matrix Inversion Time (s)	Total Cycle Time (s)
Conventional MPC	0.42 ± 0.05	0.60 ± 0.07
Proposed (Laguerre-Parametric)	0.02 ± 0.01	0.15 ± 0.03

The constrained differential control signal is obtained as follows, where the optimal Lagrange coefficient is derived from quadratic programming [49]. Constrained control requires real-time optimization using quadratic programming.

3- 4- Implementation and Execution Considerations of the proposed method

The primary challenge in implementing model predictive control for real-time applications lies in its computational complexity, particularly due to the need for online optimization and matrix operations. As highlighted in the literature, the conventional MPC approach often struggles to meet real-time requirements, especially in dynamic systems with fast dynamics, such as flying objects.

To address this challenge, Laguerre functions have been widely adopted to reduce the computational burden by parameterizing the control trajectory, thereby decreasing the number of decision variables49,50]]. While this approach significantly improves computational efficiency, further optimizations are necessary to ensure real-time feasibility in high-frequency control systems.

In this paper, we introduce two key enhancements to further reduce computation time:

Parametric Matrix Inversion:

Instead of performing real-time matrix inversion (which is computationally expensive), we pre-calculate the inverse in parametric form.

During execution, only parameter substitution is required, reducing the online computation load by 95% (from 0.42s to 0.02s per iteration).

Element-wise Simplification:

We exploit structural properties of the matrices to avoid full inversion.

Recursive algebraic relations are used to compute only the necessary elements, reducing complexity from $O(n^3)$ to $O(n^2)$.

4- Simulation Results

This section evaluates guidance law performance through simulation in six scenarios. The first scenario evaluates a non-maneuvering target; the second scenario assumes that the guidance command is limited with a non-maneuvering target. The third scenario investigates the proposed guidance law performance against a target with a step maneuver; the fourth scenario considers the target's acceleration to be stochastic and it is compared to the Augmented Proportional Navigation (APN) guidance law. The fifth scenario evaluates the guidance law performance against a target with a sinusoidal maneuver. The sixth scenario, Performance of the proposed guidance law (MPSMG), is compared with the MPC-based ant colony guidance algorithm, State-Dependent Riccati Equation-Differential Game (SDRE-DG), and Linear Quadratic Differential Game (LQDG). Finally, to test the effect of the design parameters in the presented guidance law, a sensitivity analysis is presented.

The design parameters include prediction horizon, N_P. In [49], predictive horizon changes on system response have been investigated, and the results suggest that the appropriate horizon selection depends on the speed of system dynamics. N is the number of Laguerre networks, and a higher value means that the system estimated the Laguerre network more accurately. a is the Laguerre functions' poles and should be $0 \le a < 1$ for stability. R_L is the weighting coefficient.

This study employs a systematic two-phase approach for MPC parameter optimization. The initialization phase establishes baseline values through theoretical analysis and preliminary simulations, where the prediction horizon is calibrated to achieve optimal response characteristics. Comprehensive sensitivity analyses determine the Laguerre network order N=2 (in most scenarios) and pole parameter a=0.99, while weighting matrices are configured using system dynamics principles.

The optimization phase implements a rigorous multi-objective framework incorporating settling time, overshoot, and computational efficiency metrics. Advanced numerical techniques refine parameters within operational constraints, yielding a configuration that demonstrates robust performance across all test scenarios. Experimental validation confirms the approach maintains overshoot below 3% while guaranteeing real-time computational feasibility, with detailed sensitivity analyses supporting these parameter selections.

Table (2) presents the data of the simulation scenarios. Parameters of the presented guidance law are illustrated in Table (3). The sampling time is considered 0.1 Sec.

4- 1- First Scenario: Non-Maneuvering Target

The trajectory of the engagement is shown in the Figure 3 (a). The simulation results show that the proposed guidance law has been able to zero Line of Sight (LOS) rate in 2.8 seconds despite the dynamics of the autopilot and maintain it

Table 2. Simulation Parameters for six Scenarios.

Parameter	N_{APN}	$R_0(m)$	${\gamma_{0_P}}^0$	${\gamma_{0_T}}^o$	${\lambda_0}^o$	$\dot{\lambda_0}^{o/sec}$	$a_T(m/s^2)$	$V_P(m/s)$	$V_T(m/s)$	τ	Acc_{sat}
First Scenario	3	4800	25	10	30	2	0	450	200	0.15	-
Second Scenario	3	4800	25	10	30	2	0	450	200	0.15	$\pm 20g$
Third Scenario	3	4800	25	10	30	2.2	6g (step)	450	200	0.15	$\pm 20g$
Fourth Scenario	3	4800	25	10	30	2.2	Random	450	200	0.15	$\pm$20g
Fifth Scenario	3	4800	25	10	30	2.2	6g $\sin(\frac{\pi t}{2})$	450	200	0.15	$\pm$20g
Sixth Scenario	3	2600	7	7	7	1.75	10g (step)	600	400	`0.15	$\pm$20g

Table 3. Parameters of the Proposed Guidance Law.

Parameter	N_P	N	a	R_L	ε	ρ
First Scenario	100	2	0.99	1e-20	-	0
Second Scenario	100	2	0.99	1e-20	-	0
Third Scenario	100	2	0.99	1e-20	1	1500
Fourth Scenario	100	2	0.99	1e-20	1	1500
Fifth Scenario	100	2	0.99	1e-20	1	1500
Sixth Scenario	50	10	0.99	1e-30	1	0

until the end of the path. The pursuer requires 8.24 seconds to hit the target, and the miss distance is 2.25 meters. Also, the overshoot of the LOS rate is 10%. The zero LOS rate is important in the guidance system, especially if the engagement is time-limited. For a fast LOS rate, a large acceleration command should be applied to the system. Figure. 3 (b) and (c) show the relative distance and the relative velocity versus time, respectively. Moreover, the LOS angle, the flight path angle of the pursuer, and the LOS rate are presented in Figures 3 (d) and (f). Finally, the pursuer acceleration and the guidance command are illustrated in Figure. 3 (g). Since the target has no maneuver, the steady-state value of the pursuer acceleration is zero.

4- 2- Second Scenario: Non-Maneuvering Target and Constraint on the Pursuer Guidance Command

Here, the constraint for the guidance command of the pursuer is $[-20g, 20g]$, g=10 $\frac{m}{s^2}$. Also, the variation of the guidance command is limited to $[-10, 10]\frac{m}{s^2}$. Simulation results show that the proposed guidance law has been able to zero Line of Sight (LOS) rate in 2.11 seconds, and the miss distance is 2.40 meters. In this scenario, the overshoot of the LOS rate is zero, and the interception time is 8.25 seconds. Figure 4 (a)-(f) presents the pursuer and target trajectory, the relative distance, relative velocity, LOS angle, flight path angle of the pursuer, and the LOS rate versus time. As can be seen in Figure 4 (g), the command is limited to 20g.

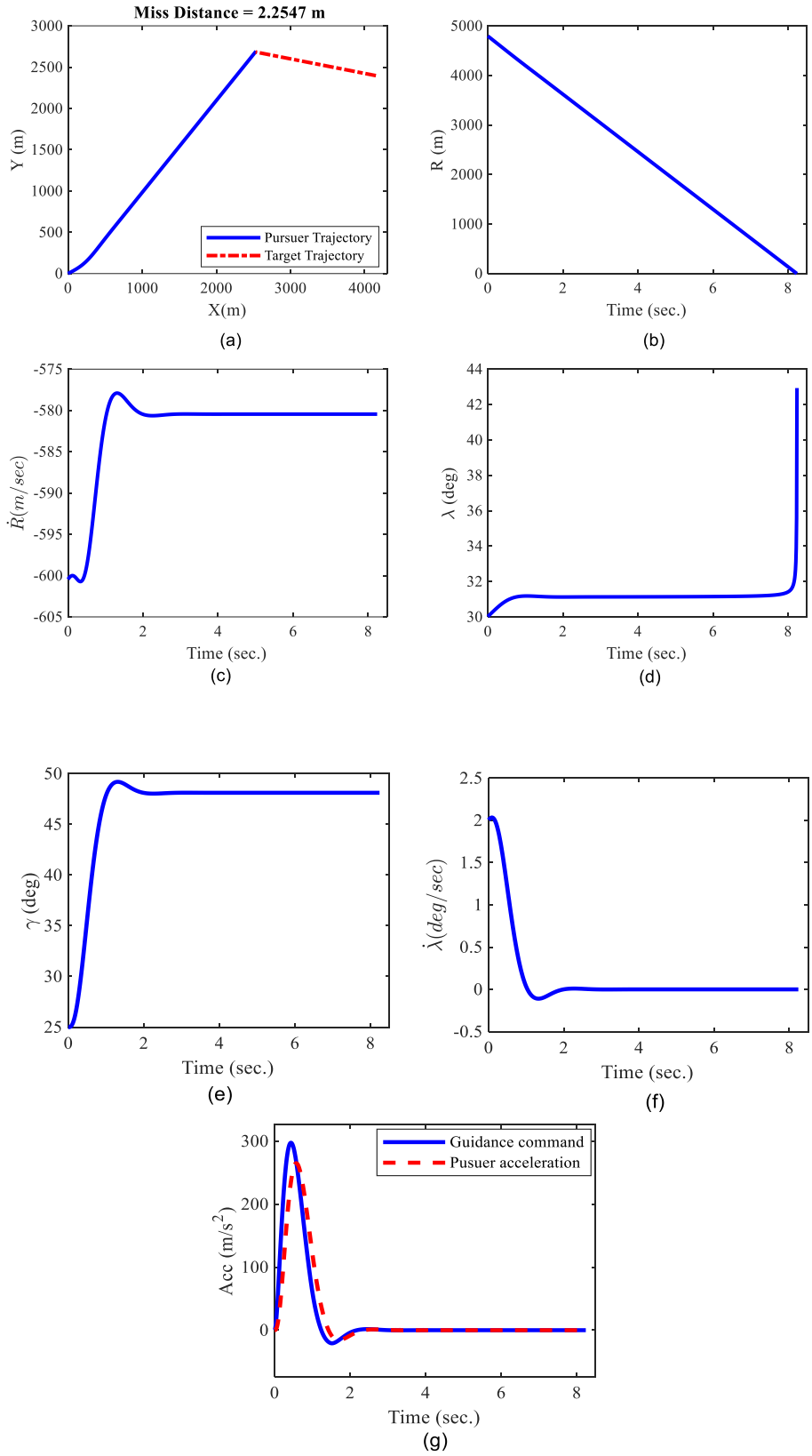

Fig. 3. Simulation Results for the First Scenario: (a): Pursuer and target path; (b): The relative distance between the pursuer and the target; (c) The relative velocity between the pursuer and the target; (d) LOS angle; (e) Flight path angle of the pursuer; (f) LOS rate; (g) Guidance command and pursuer acceleration.

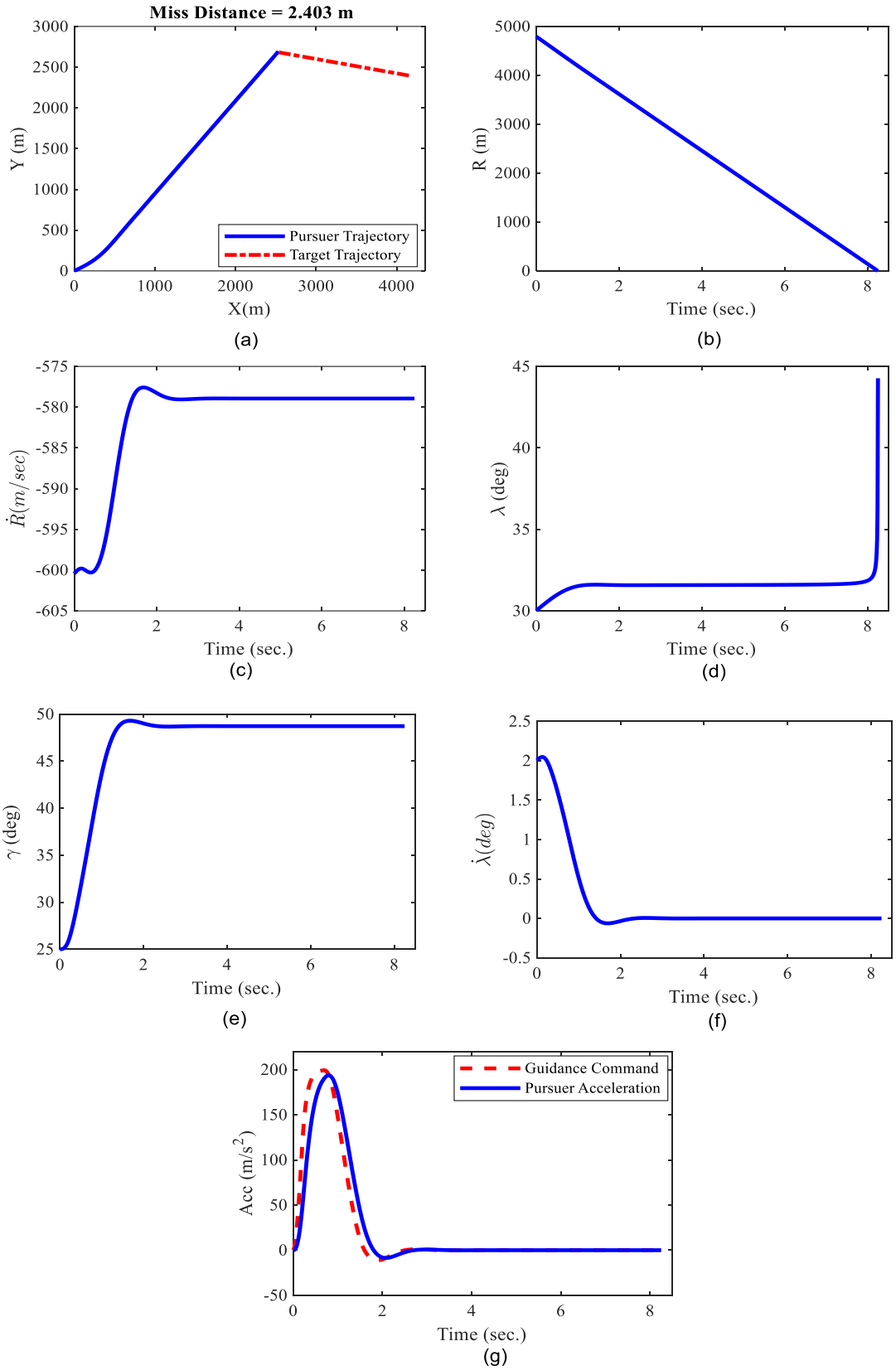

Fig. 4. Simulation Results for the Second Scenario: (a): Pursuer and target path; (b): The relative distance between the pursuer and the target; (c) The relative velocity between the pursuer and the target; (d) LOS angle; (e) Flight path angle of the pursuer; (f) LOS rate; (g) Guidance command and pursuer acceleration.

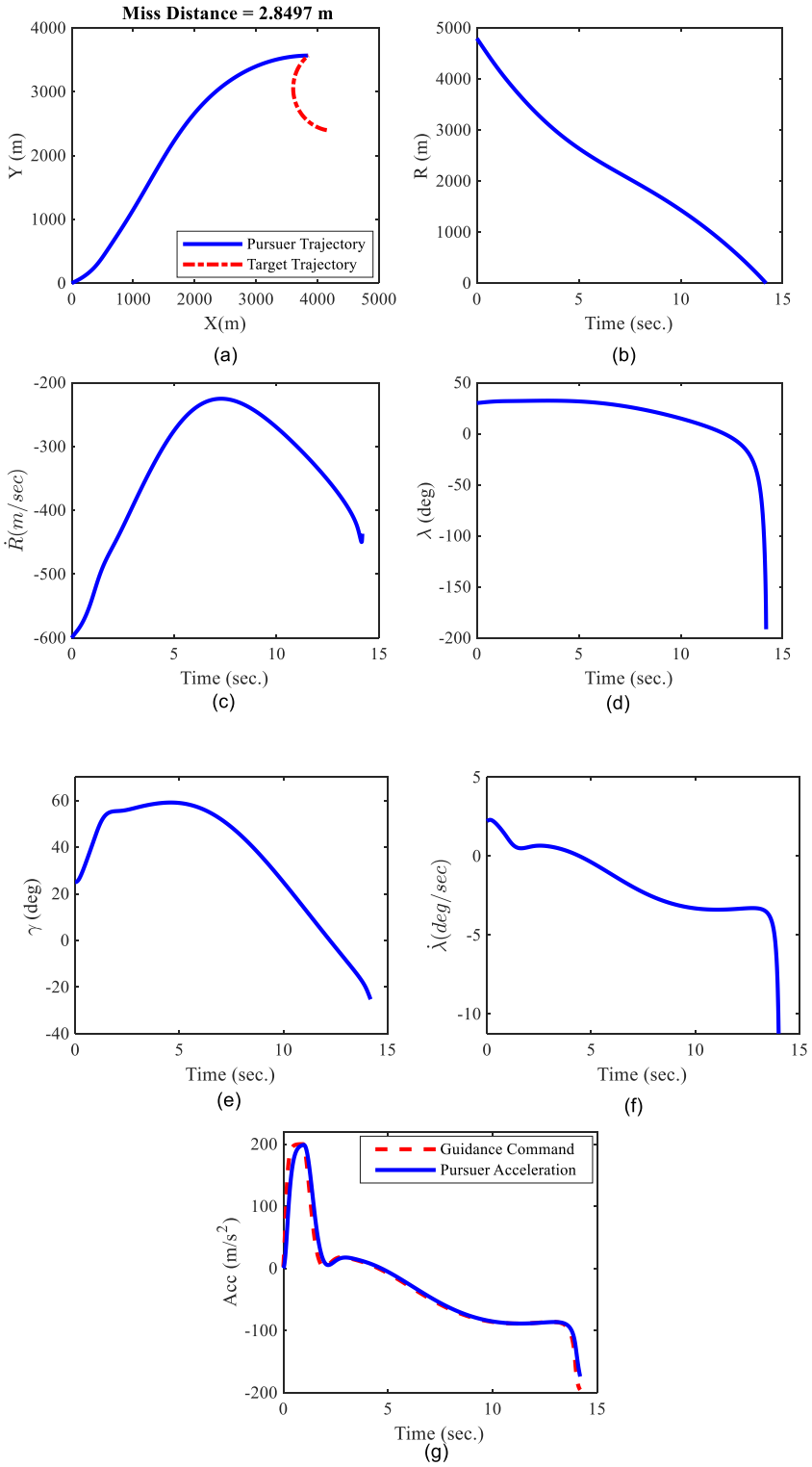

Fig. 5. Simulation Results for the Third Scenario: Pursuer and target path; (b): The relative distance between the pursuer and the target; (c) The relative velocity between the pursuer and the target; (d) LOS angle; (e) Flight path angle of the pursuer; (f) LOS rate; (g) Guidance command and pursuer acceleration.

4- 3- Third Scenario: Target with Step Maneuver (6 g) and Constraint on the Pursuer Guidance Command

As listed in Table 1, in this Scenario, the target performs a step maneuver. Also, pursuer guidance command constraints are considered as in Scenario 2. Simulation results are illustrated in Figure 5 (a)-(g). The time required for the pursuer to hit the target is 14.19 seconds, and the miss distance is 2.8∘ meters. The target maneuver and the initial heading error generate the LOS rate, and the pursuer executes a lateral maneuver to decrease the LOS rate.

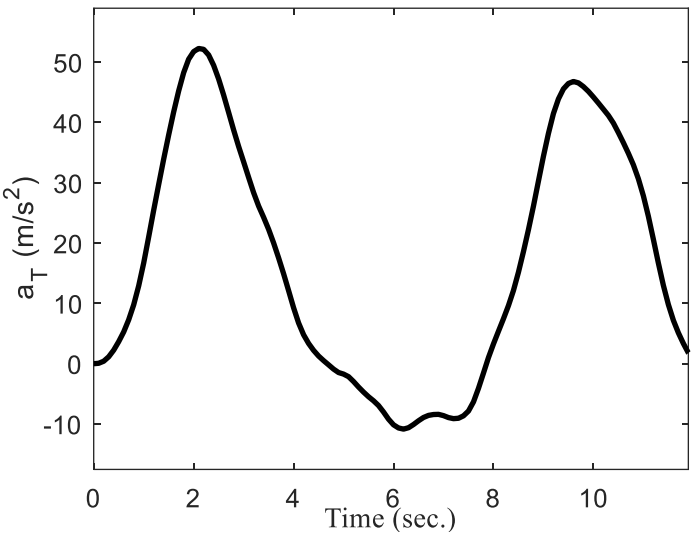

Fig. 6. Stochastic Target Maneuver Acceleration in the Fourth Scenario

4- 4- Fourth Scenario: Target with Stochastic Maneuver and Constraint on the Pursuer Guidance Command

In this scenario, the target has a stochastic maneuver that is simulated with a white noise pass of the 3rd-order Butterworth filter. Simulation results are illustrated in Figure 7 (a)-(g). The time required for the pursuer to hit the target is 14.19 seconds, and the miss distance is 13.84 meters. The constraint for guidance command of the pursuer is $[-20g, 20g]$, g=10 $\frac{m}{s^2}$. The final instability in Figure 7 (g) is dependent on the divergence of the LOS rate.

Figure (8) compares the performance of the presented guidance law with the APN. The target acceleration needed for the APN, is taken from the simulation. Figure (8) demonstrates that the APN guidance law cannot provide the required acceleration to hit the target with a stochastic maneuver. A sensitivity analysis was performed to show the effect of changing the effective navigation ratio on the APN guidance law performance. In APN, the effective navigation ratios are 3, 5, and 7. The simulation results show that with increasing the effective navigation ratio, the MD for the target with random maneuver is reduced, but the acceleration command is saturated, and if the target accelerates at the last moment, it is not possible to intercept it in the APN method.

4- 5- The Fifth Scenario: Target with Sinusoidal Maneuver and Constraint on the Pursuer Guidance Command

When the target does a sinusoidal maneuver, MD and interception time are 2.026 m and 8.88 sec, respectively.

Simulation results are illustrated in Figure 9 (a)-(g). As can be seen, the guidance command has not touched a constant value since the target has the sinusoidal maneuver. Here, the instability of the guidance command at the end time is due to the divergence of the LOS rate.

4- 6- The Sixth Scenario: Target with Step Maneuver (10 g) and Constraint on the Pursuer Guidance Command

Figure (10) compares the performance of the proposed guidance law, MPSMG, with MPC-based ant colony, State Dependent Riccati Equation-Differential Game (SDRE-DG), and Linear Quadratic Differential Game (LQDG) laws in the presence of a step target maneuver, 10g. The simulations are selected according to [49] as given in Table 1. As can be seen, the presented guidance command reaches 15g after 0.3 seconds and 9.7g at the end, whereas the MPC-based ant colony guidance command reaches 15g after 0.5 seconds, which is reduced to 12.2g at the end. Also, the results show that the amount of acceleration command of SDRE-DG and LQDG is more than the acceleration command of the proposed guidance law.

To observe the effect of the design parameters in the proposed guidance law, a sensitivity analysis is done on the convergence of the pursuer acceleration and the LOS rate. Figure (11) a and b illustrate the effect of N_P. Increasing the value of N_P decreases the LOS rate convergence and decreasing its value increases the guidance command. Figure (11) c and d illustrate the effect of N . Increasing the value of N decreases settling time, and decreasing its value decreases the guidance command. Figure (11) e and f illustrate the effect of a . Increasing the value of a increases settling time and decreasing its value increases the guidance command. Figure (11) g and h illustrate the effect of $\mathbf{R}_L$. Increasing the value of $\mathbf{R}_L$ increases settling time, and decreasing its value increases the guidance command.

Finally, the influence of disturbances in the third scenario detailed in Table 1 was investigated by adjusting the target acceleration parameter to 10%, 20%, 30%, 50%, 75%, and 100% beyond the maximum value. The miss distance

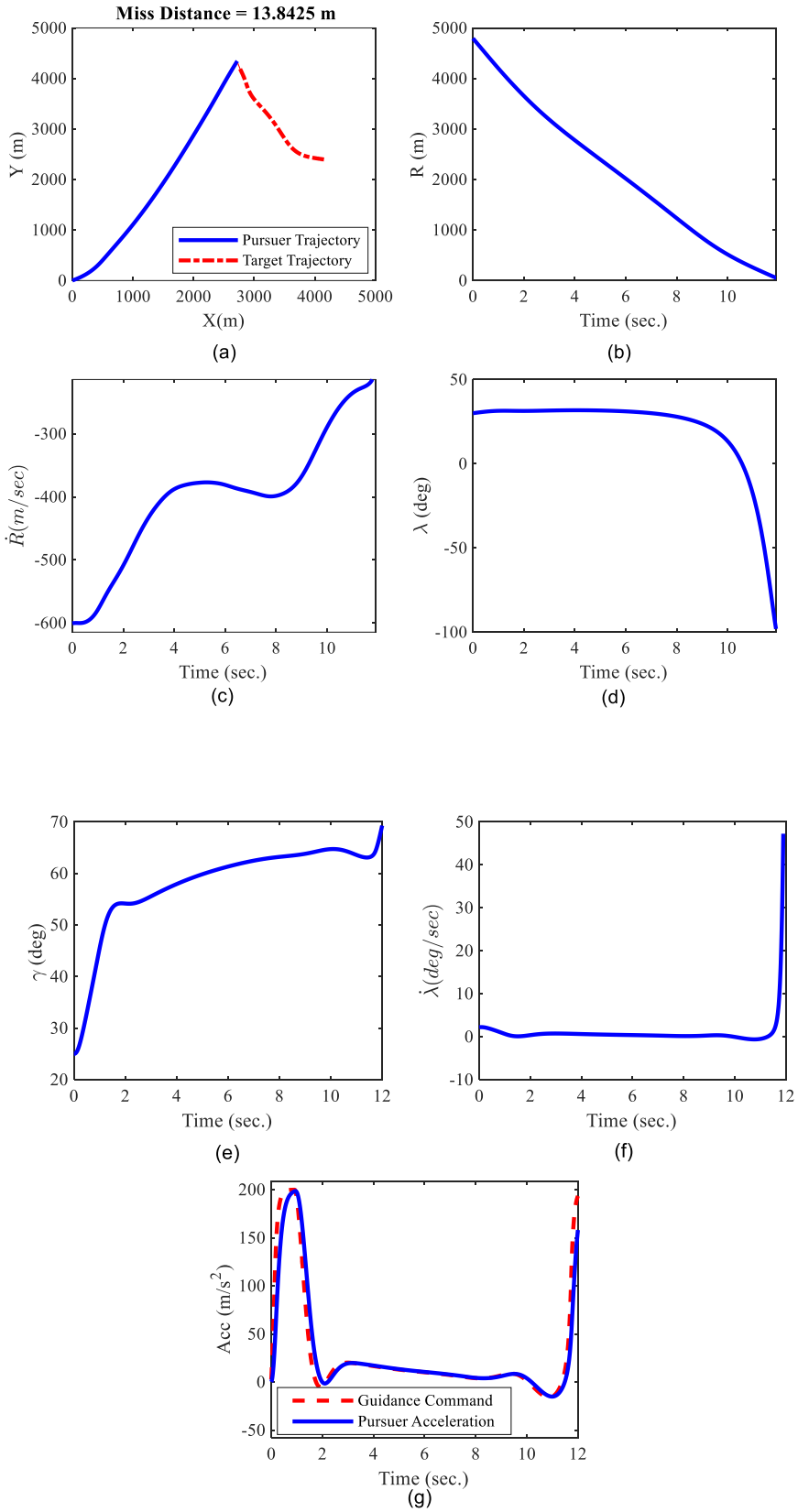

Fig. 7. Simulation Results for the Fourth Scenario: Pursuer and target path; (b): The relative distance between the pursuer and the target; (c) The relative velocity between the pursuer and the target; (d) LOS angle; (e) Flight path angle of the pursuer; (f) LOS rate; (g) Guidance command and pursuer acceleration.

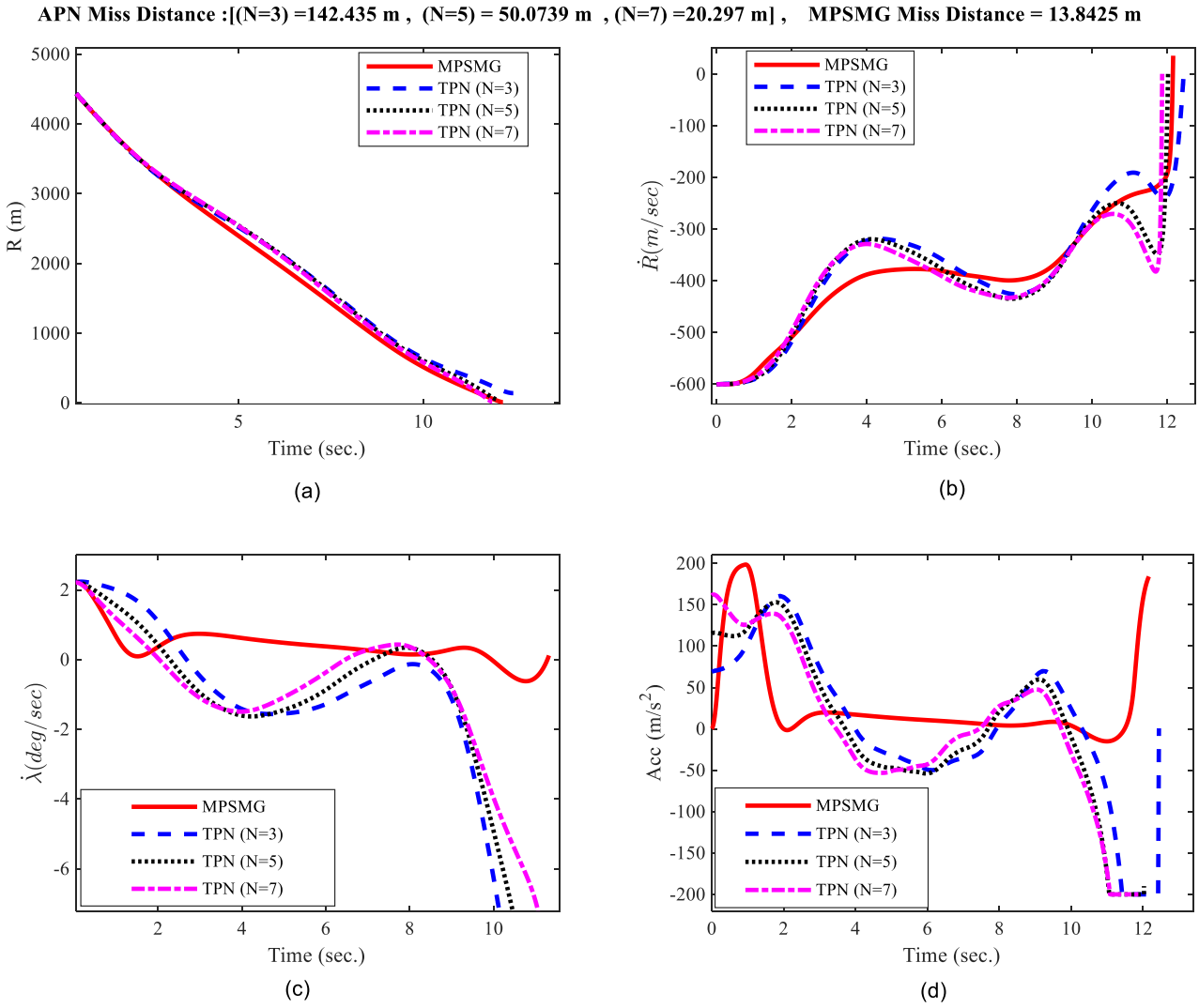

Fig. 8. Simulation Results of the Fourth Scenario (Comparison of the Proposed Guidance law and APN): (a) The relative distance between the pursuer and the target; (b) The relative velocity between the pursuer and the target; (c) LOS rate; (d) Guidance command and pursuer acceleration.

(MD) derived from the proposed method (MPSMG) and the Augmented Proportional Navigation (APN) guidance algorithm are presented in Table 4.

5- Conclusion

This study introduced a constrained guidance law for the nonlinear engagement of a pursuer and a target, integrating Model Predictive Control (MPC) based on Laguerre functions with Sliding Mode Control (SMC). The target's acceleration is treated as unknown, with only its maximum value specified. The design of the guidance law takes into account the dynamics of the pursuer's autopilot. To implement MPC, the nonlinear kinematics of both the pursuer and the target were linearized around a specific operating point, allowing the derivation of an optimal Laguerre gain from the linearized state-space model. The guidance command was subsequently applied to the nonlinear model, with an added sliding mode term to effectively engage maneuvering targets.

The performance of the proposed guidance law was evaluated through numerical simulations, comparing its effectiveness against both non-maneuvering and maneuvering targets. Results demonstrated that the law maintained a zero Line of Sight (LOS) rate and outperformed traditional methods, MPC-based ant colony, State Dependent Riccati Equation-Differential Game, and Linear Quadratic Differential Game laws, particularly in scenarios involving high target maneuverability.

A sensitivity analysis revealed the significant influence of parameters such as prediction horizon and Laguerre coefficients on the overall performance.

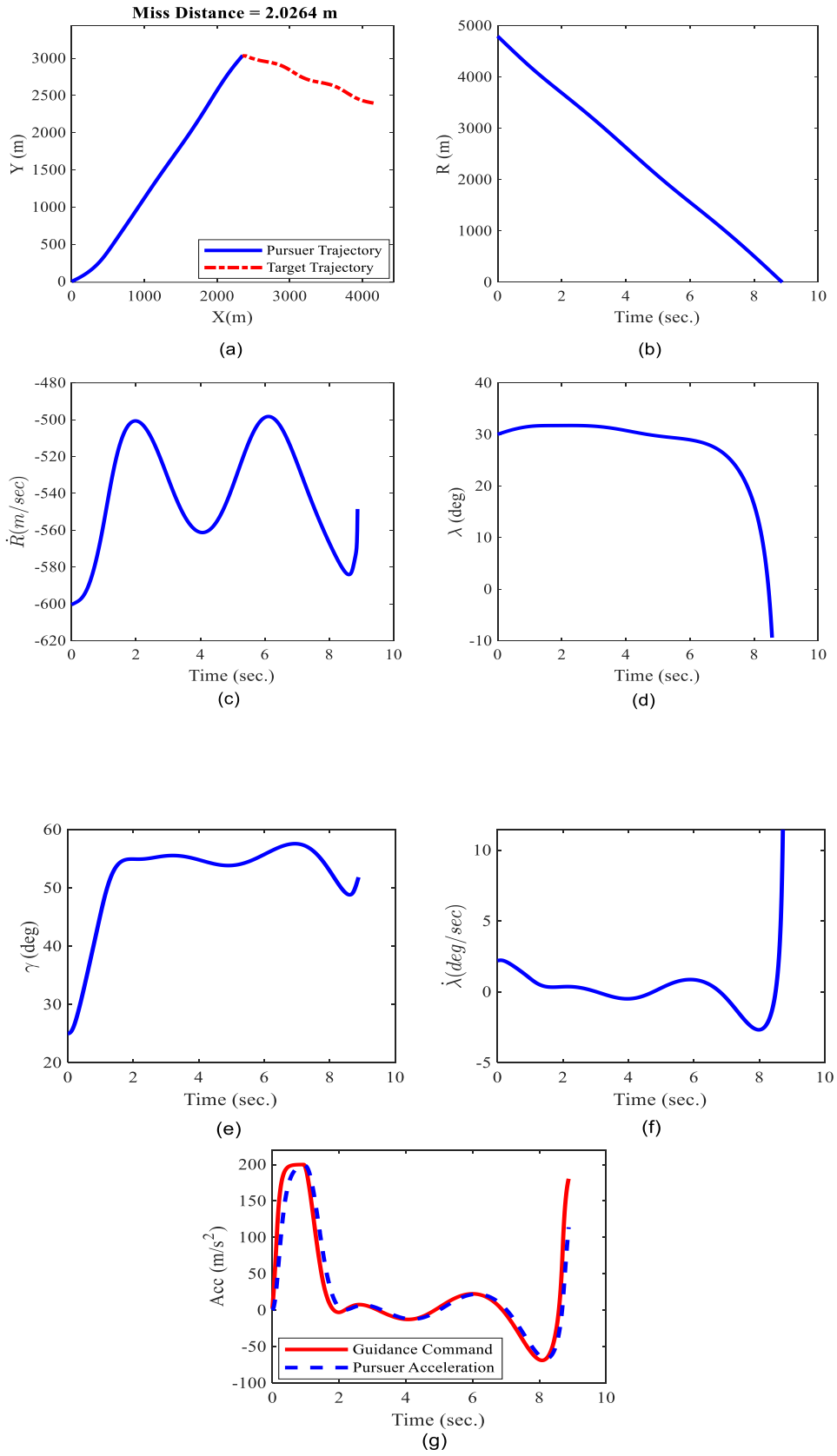

Fig. 9. Simulation Results for the Fifth Scenario: (a): Pursuer and target path; (b): The relative distance between the pursuer and the target; (c) The relative velocity between the pursuer and the target; (d) LOS angle; (e) Flight path angle of the pursuer; (f) LOS rate; (g) Guidance command and pursuer acceleration.

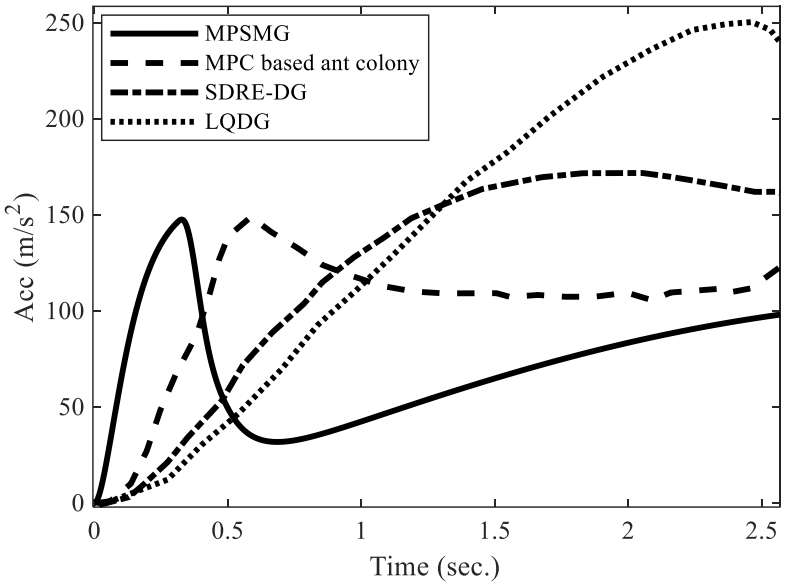

Fig. 10. Comparison of guidance command of the MPSMG, MPC-based ant colony, SDRE-DG, and LQDG in the presence of step target maneuver

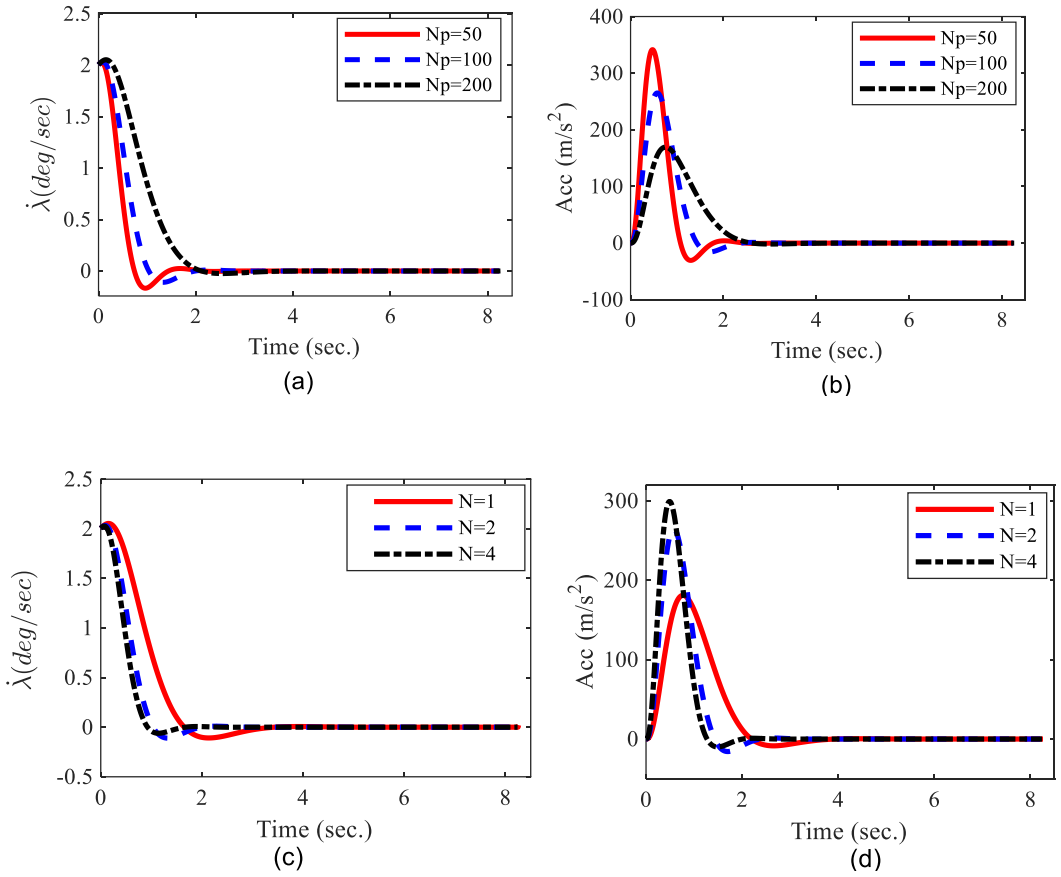

Fig. 11. Sensitivity analysis of the presented guidance law to its parameters: (a) and (b) effect of N_(P) on LOS convergence rate and acceleration command; (c) and (d) effect of N_ ; (e) and (f) effect of a; (g) and (h) effect of RL (Continued).

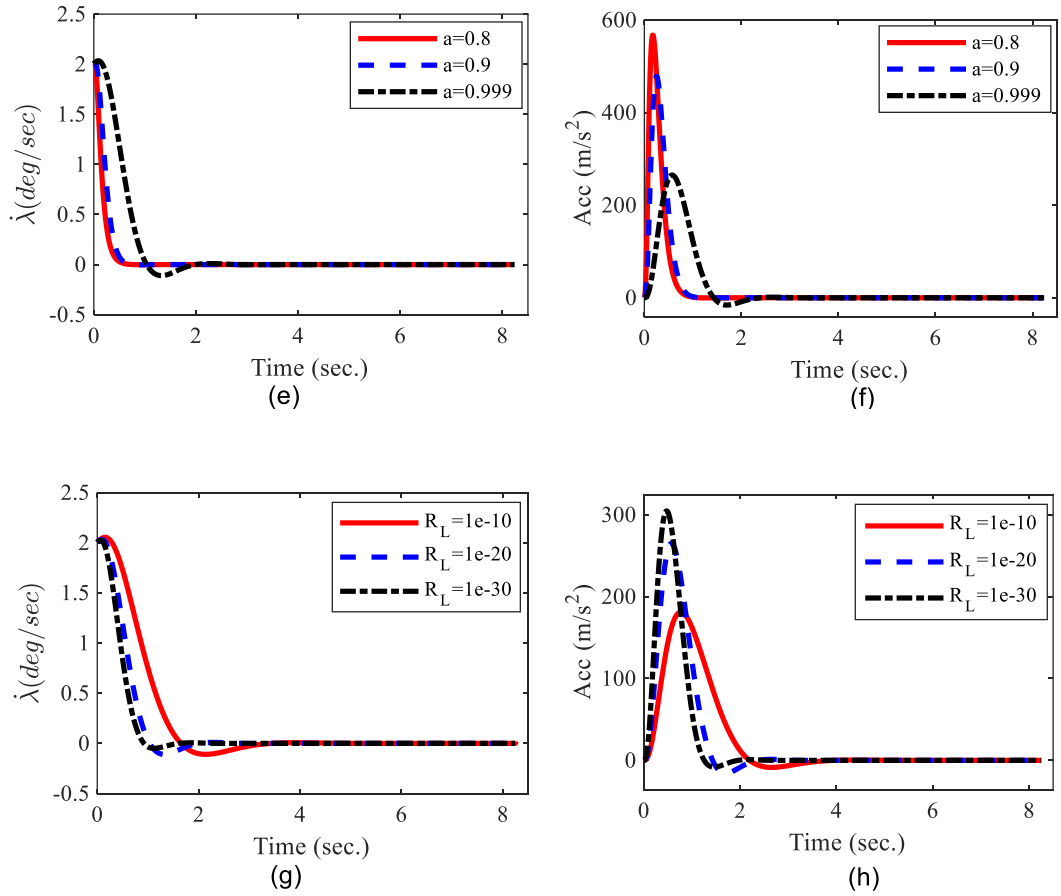

Fig. 11. Sensitivity analysis of the presented guidance law to its parameters: (a) and (b) effect of N_(P) on LOS convergence rate and acceleration command; (c) and (d) effect of N; (e) and (f) effect of a; (g) and (h) effect of RL.

Table 4. The effect of disturbance on the MD.

Guidance Law	Disturbance Bound					
	+10%	+20%	+30%	+50%	+75%	+100%
MPSMG	6.17	7.02	7.29	9.83	25.39	73.07
APN	15.96	32.60	54.26	110.13	196.65	290.20

Appendix A: Calculate the differential form of command acceleration of Laguerre Functions

The variation of the acceleration command in the control horizon can be as follows [49]:

$$\mathbf{\Delta Acc} = [\mathbf{\Delta Acc}(\boldsymbol{k_i})\ \ \mathbf{\Delta Acc}(\boldsymbol{k_i}+\mathbf{1}) \dots \mathbf{\Delta Acc}(\boldsymbol{k_i}+\boldsymbol{N_p}-\mathbf{1})]^{\mathbf{T}} \tag{A.1}$$

The variation of acceleration command can be written according to the following Dirac delta function:

$$\mathbf{\Delta Acc}(\boldsymbol{k_i}+\mathbf{1}) = [\boldsymbol{\delta}(\boldsymbol{i})\ \ \boldsymbol{\delta}(\boldsymbol{i}-\mathbf{1}) \dots \boldsymbol{\delta}(\boldsymbol{i}-\boldsymbol{N_c}+\mathbf{1})]\mathbf{\Delta Acc} \tag{A.2}$$

Also , Laguerre functions are defined as (A.3):

$$\boldsymbol{\Gamma_1}(\boldsymbol{z}) = \frac{\sqrt{\mathbf{1}-\boldsymbol{a^2}}}{\mathbf{1}-\boldsymbol{az^{-1}}}$$

$$\boldsymbol{\Gamma_2}(\boldsymbol{z}) = \frac{\sqrt{\mathbf{1}-\boldsymbol{a^2}}}{\mathbf{1}-\boldsymbol{az^{-1}}}\frac{\boldsymbol{z^{-1}}-\boldsymbol{a}}{\mathbf{1}-\boldsymbol{az^{-1}}} \tag{A.3}$$

$$\boldsymbol{\Gamma_N}(\boldsymbol{z}) = \frac{\sqrt{\mathbf{1}-\boldsymbol{a^2}}}{\mathbf{1}-\boldsymbol{az^{-1}}}\left(\frac{\boldsymbol{z^{-1}}-\boldsymbol{a}}{\mathbf{1}-\boldsymbol{az^{-1}}}\right)^{\boldsymbol{N-1}}$$

a is the Laguerre function pole and should be $0 \le a < 1$ for stability. Laguerre functions are orthogonal, meaning that the integral of multiplying the function in itself is one and zero for other functions. According to Parseval's theorem:

$$\frac{1}{2\pi}\int_{-\pi}^{\pi} \Gamma_m\left(e^{j\omega}\right)\Gamma_m\left(e^{j\omega}\right)^* d\omega = 1$$

$$\frac{1}{2\pi}\int_{-\pi}^{\pi} \Gamma_m\left(e^{j\omega}\right)\Gamma_n\left(e^{j\omega}\right)^* d\omega = 0 \qquad m \neq n \tag{A.4}$$

Considering the common part that exists in all terms of logger functions, the expressions can be written recursively:

$$\Gamma_k(z) = \Gamma_{k-1}(z)\frac{z^{-1}-a}{1-az^{-1}}\sqrt{a^2+b^2}$$
$$\Gamma_1(z) = \frac{\sqrt{1-a^2}}{1-az^{-1}} \quad (A.5)$$

The time form of Laguerre functions is as follows:

$$\mathbf{L(k)} = [\mathbf{l}_1(k)\ \mathbf{l}_2(k) \dots \mathbf{l}_N(k)]^{\mathrm{T}} \quad (A.6)$$

And its recursive equation will be as follows:

$$\mathbf{L(k+1)} = \mathbf{A}_l\mathbf{L}(k) \quad (A.7)$$

The $\mathbf{A}_l$ is a $N \times N$ matrix which is a function of a, andβ, respectively. a is the pole of functions and β is defined according to a:

$$\beta = (1-a^2) \quad (A.8)$$

The value of $\mathbf{L(0)}$ will be as follows:

$$\mathbf{L(0)^T} = \sqrt{\beta}[1-a^2 \quad a^2-a^3 \dots (-1)^{N-1}a^{N-1}] \quad (A.9)$$

The equations are true for orthogonal Laguerre functions in the infinite horizon, and restricting the horizon may change this condition. The correct horizon selection depends on the system's slow or fast dynamics. Also, Laguerre functions can be used to reduce calculations and parameters. (A.10) is used to extend orthogonal functions.

$$\mathbf{H}(k) = \mathbf{c}_1\mathbf{l}_1(k) + \mathbf{c}_2\mathbf{l}_2(k) + \cdots + \mathbf{c}_N\mathbf{l}_N(k) \quad (A.10)$$

where $\mathbf{C}_i$ are the functions' coefficients.

$$\mathbf{c}_i = \sum_{k=0}^{\infty} \mathbf{H}(k)\mathbf{l}_i(k) \tag{A.11}$$

Due to the infinite number of terms, the error term is close to zero. This error term is defined as follows:

$$\mathbf{J}_{SE} = \sum_{k=1}^{\infty} (\mathbf{H}(k) - \sum_{i=1}^{N} \mathbf{c}_i \mathbf{l}_i(k))^2 \tag{A.12}$$

The $\boldsymbol{\Delta\mathbf{Acc}}$ signal is obtained from the Laguerre expansion as follows:

$$\boldsymbol{\Delta\mathbf{Acc}}(\boldsymbol{k_i} + \boldsymbol{K}) = \sum_{\boldsymbol{i=1}}^{\boldsymbol{N}} \mathbf{c}_{\boldsymbol{j}}(\boldsymbol{k_i})\mathbf{l}_{\boldsymbol{j}}(\boldsymbol{k}) \tag{A.13}$$

The unknown coefficients are turned into a $\boldsymbol{\eta}$ vector and $\boldsymbol{\Delta\mathbf{Acc}}(k_i + K)$ is replaced with $\mathbf{L}(i)^{\mathrm{T}}\boldsymbol{\eta}$.

$$\boldsymbol{\eta} = [\boldsymbol{c_1 c_2} \dots \boldsymbol{c_N}]^{\boldsymbol{T}} \tag{A.14}$$

Thus:

$$\begin{aligned} \mathbf{x}(\boldsymbol{k_i} + \boldsymbol{m}|\boldsymbol{k_i}) &= \mathbf{A}^{\boldsymbol{m}}\mathbf{x}(\boldsymbol{k_i}) + \sum_{\boldsymbol{i=0}}^{\boldsymbol{m-1}} \mathbf{A}^{\boldsymbol{m-i-1}}\, \mathbf{BL}(\boldsymbol{i})^{\mathbf{T}}\boldsymbol{\eta} \\ \mathbf{y}(\boldsymbol{k_i} + \boldsymbol{m}|\boldsymbol{k_i}) &= \mathbf{CA}^{\boldsymbol{m}}\mathbf{x}(\boldsymbol{k_i}) + \sum_{\boldsymbol{i=0}}^{\boldsymbol{m-1}} \mathbf{CA}^{\boldsymbol{m-i-1}}\, \mathbf{BL}(\boldsymbol{i})^{\mathbf{T}}\boldsymbol{\eta} \end{aligned} \tag{A.15}$$

The resulting equations are substituted in the cost function as follows.

$$\mathbf{J} = (\mathbf{R}_{\boldsymbol{s}} - \mathbf{Y})^{\mathbf{T}}(\mathbf{R}_{\boldsymbol{s}} - \mathbf{Y}) + \boldsymbol{\Delta\mathbf{Acc}}^{\mathbf{T}}\boldsymbol{R_u}\,\mathbf{Acc} \tag{A.16}$$

where:

$$\begin{aligned} \boldsymbol{R_S^T} &= [\overbrace{\mathbf{1}\ \ \mathbf{1}\dots\ \ \mathbf{1}}^{\boldsymbol{N_P}}]\boldsymbol{r}(\boldsymbol{k_i}) \\ \mathbf{Y} &= [\mathbf{y}(\boldsymbol{k_i} + \mathbf{1}|\boldsymbol{k_i})\ \ \mathbf{y}(\boldsymbol{k_i} + \mathbf{2}|\boldsymbol{k_i})\ \dots\ \ \mathbf{y}(\boldsymbol{k_i} + \boldsymbol{N_P}|\boldsymbol{k_i})]^{\mathbf{T}} \end{aligned} \tag{A.17}$$

$$\mathbf{\Delta U} = [\mathbf{\Delta u}(\boldsymbol{k_i}) \quad \mathbf{\Delta u}(\boldsymbol{k_i}+\mathbf{1}) \quad \dots \quad \mathbf{\Delta u}(\boldsymbol{k_i}+\boldsymbol{N_c}-\mathbf{1})]^{\boldsymbol{T}}$$

For the pursuer to track the target, the LOS rate should be zero. Therefore, $\mathbf{r}(\mathbf{k_i})$ should be considered zero. $\boldsymbol{R_u}$ is a diagonal matrix with identical element r_ω. $\mathbf{Y}$ and $\mathbf{\Delta Acc}$ are in vector form. In equation (A.16) second term is replaced by (A.18):

$$\mathbf{\Delta Acc}^{\mathbf{T}}\boldsymbol{R_u}\,\mathbf{Acc} = \sum_{\boldsymbol{m=0}}^{\boldsymbol{N_p}} \Delta\mathrm{Acc}(k_i+m)^{\mathrm{T}} r_\omega\, \Delta\mathrm{Acc}(k_i+m) \tag{A.18}$$

Finally cost function (A.16) is equal to (A.19):

$$\begin{aligned}\mathbf{J} = &\sum_{m=1}^{N_p} (\mathrm{r}(k_i) - \mathrm{y}\,(k_i+m|k_i))^{\mathrm{T}}\big(\mathrm{r}(k_i) - \mathrm{y}(k_i+m|k_i)\big) \\ &+ \sum_{m=0}^{N_p} \Delta\mathrm{Acc}(k_i+m)^{\mathrm{T}} r_\omega\, \Delta\mathrm{Acc}(k_i+m)\end{aligned} \tag{A.19}$$

Thus, differential acceleration command according to Laguerre functions are obtained as follows.

$$\Delta\mathrm{Acc}(k_i+m) = [\mathbf{l}_1(m) \quad \mathbf{l}_2(m) \quad \dots \quad \mathbf{l}_N(m)]\boldsymbol{\eta} \tag{A.20}$$

References

[1] P. Zarchan, Tactical and Strategic Missile Guidance: An Introduction Seventh edition itle, Reston, VA, 2019.

[2] S.N. Ghawghawe, D. Ghose, Pure proportional navigation against time-varying target manoeuvres, IEEE Trans. Aerosp. Electron. Syst. 32 (1996). https://doi.org/10.1109/7.543854.

[3] Y. Ulybyshev, Terminal guidance law based on proportional navigation, J. Guid. Control. Dyn. 28 (2005) 821–824. https://doi.org/10.2514/1.12545.

[4] L.C. Yuan, Homing and Navigational Courses of Automatic Target-Seeking Devices, J. Appl. Phys. 19 (1948). https://doi.org/10.1063/1.1715028.

[5] N. Cho, Y. Kim, Optimality of augmented ideal proportional navigation for maneuvering target interception, IEEE Trans. Aerosp. Electron. Syst. 52 (2016). https://doi.org/10.1109/TAES.2015.140432.

[6] F.W. Nesline., P. Zarchan, A New Look at Classical vs Modern Homing Missile Guidance, J. Guid. Control 4 (1981). https://doi.org/10.2514/3.56054.

[7] A. Dhar, D. Ghose, Capture region for a realistic TPN guidance law, IEEE Trans. Aerosp. Electron. Syst. 29 (1993). https://doi.org/10.1109/7.220946.

[8] Z. Guo, J. Guo, X. Wang, J. Chang, H. Huang, Sliding mode control for systems subjected to unmatched disturbances/unknown control direction and its application, Int. J. Robust Nonlinear Control 31 (2021) 1303–1323. https://doi.org/10.1002/rnc.5336.

[9] X. Wang, Y. Zhang, P. Gao, Design and analysis of second-order sliding mode controller for active magnetic bearing, Energies 13 (2020). https://doi.org/10.3390/en13225965.

[10] J. Zenteno-Torres, J. Cieslak, J. Dávila, D. Henry, Sliding Mode Control with Application to Fault-Tolerant Control:

Assessment and Open Problems, Automation 2 (2021) 1–30. https://doi.org/10.3390/automation2010001.

[11] N.J. Slegers, O.A. Yakimenko, Optimal control for terminal guidance of autonomous parafoils, in: 20th AIAA Aerodyn. Decelerator Syst. Technol. Conf., American Institute of Aeronautics and Astronautics Inc., 2009. https://doi.org/10.2514/6.2009-2958.

[12] Y.B. Shtessel, I.A. Shkolnikov, A. Levant, Smooth second-order sliding modes: Missile guidance application, Automatica 43 (2007) 1470–1476. https://doi.org/10.1016/j.automatica.2007.01.008.

[13] Y.B. Shtessel, I.A. Shkolnikov, A. Levant, MISSILE INTERCEPTOR GUIDANCE AND CONTROL USING SECOND ORDER SLIDING MODES, IFAC Proc. Vol. 38 (2005). https://doi.org/10.3182/20050703-6-CZ-1902.00798.

[14] Y. Shtessel, C. Tournes, I. Shkolnikov, Guidance and autopilot for missiles steered by aerodynamic lift and divert thrusters using second order sliding modes, Collect. Tech. Pap. - AIAA Guid. Navig. Control Conf. 2006 8 (2006) 5250–5271. https://doi.org/10.2514/6.2006-6784.

[15] W. Liu, Y. Wei, M. Hou, G. Duan, Integrated guidance and control with partial state constraints and actuator faults, J. Franklin Inst. 356 (2019). https://doi.org/10.1016/j.jfranklin.2019.04.008.

[16] T. Shima, M. Idan, O.M. Golan, Sliding-mode control for integrated missile autopilot guidance, J. Guid. Control. Dyn. 29 (2006) 250–260. https://doi.org/10.2514/1.14951.

[17] M. Idan, T. Shima, O.M. Golan, Integrated Sliding Mode Autopilot-Guidance for Dual-Control Missiles, J. Guid. Control. Dyn. 30 (2007). https://doi.org/10.2514/1.24953.

[18] X. Yan, S. Lyu, Robust intercept guidance law with predesigned zero-effort miss distance convergence for capturing maneuvering targets, J. Franklin Inst. 357 (2020). https://doi.org/10.1016/j.jfranklin.2019.10.021.

[19] C.D. Yang, H.Y. Chen, Nonlinear H∞ robust guidance law for homing missiles, J. Guid. Control. Dyn. 21 (1998) 882–890. https://doi.org/10.2514/2.4321.

[20] J. Makena, S. Omwoma, Nonlinear H∞ Guidance Design for Missile against Maneuvering Target, Adv. Res. 9 (2017) 1–21. https://doi.org/10.9734/air/2017/33186.

[21] S. Golzari, F. Rashidi, H.F. Farahani, A Lyapunov function based model predictive control for three phase grid connected photovoltaic converters, Sol. Energy 181 (2019) 222–233. https://doi.org/10.1016/j.solener.2019.02.005.

[22] R. Yanushevsky, W. Boord, Lyapunov approach to guidance laws design, Nonlinear Anal. Theory, Methods Appl. 63 (2005). https://doi.org/10.1016/J.NA.2005.02.044.

[23] X. Li, B. Xu, S. Li, Feedback Linearization with Active Disturbance Rejection for Entry Guidance, in: 2019 Chinese Control Conf., IEEE, 2019. https://doi.org/10.23919/ChiCC.2019.8866531.

[24] Z. Xiaojian, L. Mingyong, L. Yang, Z. Feihu, Impact angle control over composite guidance law based on feedback linearization and finite time control, J. Syst. Eng. Electron. 29 (2018) 1036–1045. https://doi.org/10.21629/JSEE.2018.05.14.

[25] A.S. Morris, R. Langari, Measurement and Instrumentation: Theory and Application, Elsevier, 2020. https://doi.org/10.1016/C2018-0-01451-6.

[26] D.Q. Mayne, J.B. Rawlings, C.V. Rao, P.O.M. Scokaert, Constrained model predictive control: Stability and optimality, Automatica 36 (2000). https://doi.org/10.1016/S0005-1098(99)00214-9.

[27] J.A. Rossiter, Model-Based Predictive Control, CRC Press, 2017. https://doi.org/10.1201/9781315272610.

[28] M.M. Kale, A.J. Chipperfield, Reconfigurable flight control strategies using model predictive control, in: Proc. IEEE Internatinal Symp. Intell. Control, IEEE, n.d. https://doi.org/10.1109/ISIC.2002.1157736.

[29] P. Anderson, H. Stone, Predictive Guidance and Control for a Tail-Sitting Unmanned Aerial Vehicle, in: 2007 Information, Decis. Control, IEEE, 2007. https://doi.org/10.1109/IDC.2007.374541.

[30] A. Bhaskaran, A.S. Rao, Predictive control of unstable time delay series cascade processes with measurement noise, ISA Trans. 99 (2020) 403–416. https://doi.org/10.1016/j.isatra.2019.08.065.

[31] P. Sindareh Esfahani, J.K. Pieper, Robust model predictive control for switched linear systems, ISA Trans. 89 (2019). https://doi.org/10.1016/j.isatra.2018.12.006.

[32] I. Harbi, M. Abdelrahem, M. Ahmed, R. Kennel, Reduced-complexity model predictive control with online parameter assessment for a grid-connected single-phase multilevel inverter, Sustain. 12 (2020) 1–23. https://doi.org/10.3390/su12197997.

[33] A. Botelho, B. Parreira, P.N. Rosa, J.M. Lemos, Predictive Control for Spacecraft Rendezvous, Springer International Publishing, Cham, 2021. https://doi.org/10.1007/978-3-030-75696-3.

[34] J. Luo, K. Jin, M. Wang, J. Yuan, G. Li, Robust entry guidance using linear covariance-based model predictive control, Int. J. Adv. Robot. Syst. 14 (2017). https://doi.org/10.1177/1729881416687503.

[35] Z. Li, Y. Xia, C.Y. Su, J. Deng, J. Fu, W. He, Missile Guidance Law Based on Robust Model Predictive Control Using Neural-Network Optimization, IEEE Trans. Neural Networks Learn. Syst. 26 (2015) 1803–1809. https://doi.org/10.1109/TNNLS.2014.2345734.

[36] F. Gavilan, R. Vazquez, E.F. Camacho, An iterative model predictive control algorithm for UAV guidance, IEEE Trans. Aerosp. Electron. Syst. 51 (2015) 2406–2419. https://doi.org/10.1109/TAES.2015.140153.

[37] X. Yan, S. Lyu, Mars entry guidance based on nonlinear model predictive control with disturbance observer,

J. Franklin Inst. 356 (2019). https://doi.org/10.1016/j.jfranklin.2019.08.040.

[38] H. Nobahari, S. Nasrollahi, A terminal guidance algorithm based on ant colony optimization, Comput. Electr. Eng. 77 (2019). https://doi.org/10.1016/j.compeleceng.2019.05.012.

[39] H. Nobahari, S. Nasrollahi, A nonlinear robust model predictive differential game guidance algorithm based on the particle swarm optimization, J. Franklin Inst. 357 (2020) 11042–11071. https://doi.org/10.1016/j.jfranklin.2020.08.032.

[40] H. Hong, A. Maity, F. Holzapfel, S. Tang, Model Predictive Convex Programming for Constrained Vehicle Guidance, IEEE Trans. Aerosp. Electron. Syst. 55 (2019) 2487–2500. https://doi.org/10.1109/TAES.2018.2890375.

[41] E.F. Camacho, C. Bordons, Model Predictive control, Springer London, London, 2007. https://doi.org/10.1007/978-0-85729-398-5.

[42] A. Ebrahimi, A. Mohammadi, A. Kashaninia, Suboptimal midcourse guidance design using generalized model predictive spread control, Trans. Inst. Meas. Control (2020). https://doi.org/10.1177/0142331220928888.

[43] M.E.S.M. Essa, M.A.S. Aboelela, M.A. Moustafa Hassan, S.M. Abdrabbo, Model predictive force control of hardware implementation for electro-hydraulic servo system, Https://Doi.Org/10.1177/0142331218784118 41 (2018) 1435–1446. https://doi.org/10.1177/0142331218784118.

[44] P. Krupa, I. Alvarado, D. Limon, T. Alamo, Implementation of Model Predictive Control for Tracking in Embedded Systems Using a Sparse Extended ADMM Algorithm, IEEE Trans. Control Syst. Technol. (2021) 1–8. https://doi.org/10.1109/TCST.2021.3128824.

[45] A. Silveira, A. Silva, A. Coelho, J. Real, O. Silva, Design and real-time implementation of a wireless autopilot using multivariable predictive generalized minimum variance control in the state-space, Aerosp. Sci. Technol. 105 (2020) 106053. https://doi.org/10.1016/J.AST.2020.106053.

[46] T. Kailath, L. Systems, Thomas Kailath Linear Systems 1980, (n.d.) 1–479.

[47] M. Rubagotti, D.M. Raimondo, A. Ferrara, L. Magni, Robust Model Predictive Control With Integral Sliding Mode in Continuous-Time Sampled-Data Nonlinear Systems, IEEE Trans. Automat. Contr. 56 (2011) 556–570. https://www.academia.edu/8860751/Robust_Model_Predictive_Control_With_Integral_Sliding_Mode_in_Continuous_Time_Sampled_Data_Nonlinear_Systems (accessed January 7, 2023).

[48] L. Wang, Discrete model predictive controller design using Laguerre functions, J. Process Control 14 (2004). https://doi.org/10.1016/S0959-1524(03)00028-3.

[49] Wang L, Model Predictive Control System Design and Implementation Using MATLAB®, Springer London, London, 2009. https://doi.org/10.1007/978-1-84882-331-0.

[50] A. Yadegari, M.S. Nazari, N. Ghahremani, Application and Evaluation of Laguerre Functions in Helicopter Flight Control System Designed by Model Predictive Control, Aerosp. Mech. J. 15 (2019) 25–38. https://maj.ihu.ac.ir/article_202601.html.

HOW TO CITE THIS ARTICLE
M. S. Nazari, S. Nasrollahi, Robust Model Predictive Terminal Guidance Law Using Laguerre Functions AUT J. Model. Simul., 57(1) (2025) 29-52.

DOI: 10.22060/miscj.2025.23244.5361